JOURNAL OF GEOPHYSICAL RESEARCH, VOL. 111, D19303, doi:10.1029/2006JD007089, 2006

Tropospheric ozone determined from Aura OMI and MLS: Evaluation of measurements and comparison with the Global Modeling Initiative's Chemical Transport Model

J. R. Ziemke,[1,2] S. Chandra,[1,2] B. N. Duncan,[1,2] L. Froidevaux,[3] P. K. Bhartia,[4] P. F. Levelt,[5] and J. W. Waters[3]

Received 19 January 2006; revised 20 April 2006; accepted 14 June 2006; published 5 October 2006.

[1] Ozone measurements from the OMI and MLS instruments on board the Aura satellite are used for deriving global distributions of tropospheric column ozone (TCO). TCO is determined using the tropospheric ozone residual method which involves subtracting measurements of MLS stratospheric column ozone (SCO) from OMI total column ozone after adjusting for intercalibration differences of the two instruments using the convective-cloud differential method. The derived TCO field, which covers one complete year of mostly continuous daily measurements from late August 2004 through August 2005, is used for studying the regional and global pollution on a timescale of a few days to months. The seasonal and zonal characteristics of the observed TCO fields are also compared with TCO fields derived from the Global Modeling Initiative's Chemical Transport Model. The model and observations show interesting similarities with respect to zonal and seasonal variations. However, there are notable differences, particularly over the vast region of the Saharan desert.

Citation: Ziemke, J. R., S. Chandra, B. N. Duncan, L. Froidevaux, P. K. Bhartia, P. F. Levelt, and J. W. Waters (2006), Tropospheric ozone determined from Aura OMI and MLS: Evaluation of measurements and comparison with the Global Modeling Initiative's Chemical Transport Model, *J. Geophys. Res.*, *111*, D19303, doi:10.1029/2006JD007089.

1. Introduction

[2] Many of the current techniques for deriving tropospheric ozone are based on the tropospheric ozone residual (TOR) method, which derives tropospheric column ozone (TCO) by subtracting concurrent measurements of stratospheric column ozone (SCO) from total column ozone measured by the Total Ozone Mapping Spectrometer (TOMS) instrument [*Fishman and Larsen*, 1987; *Fishman et al.*, 1990]. The TOR concept, which has recently been used by *Fishman et al.* [2003] using the TOMS and Solar Backscatter Ultraviolet (SBUV) combination, and by *Chandra et al.* [2003] using the TOMS and Upper Atmosphere Research Satellite (UARS) Microwave Limb Sounder (MLS) combination, has been implemented to derive TCO and SCO fields from the Aura satellite where total column ozone is measured by the Dutch-Finnish Ozone Monitoring Instrument (OMI) [*Levelt et al.*, 2006a], and SCO is measured by the MLS instrument [*Waters et al.*, 2006]. The use of MLS on board Aura for measuring SCO is a significant improvement in alleviating some of the problems associated with the use of SBUV or UARS MLS. The SBUV measurements have difficulty in retrieving ozone in the lower stratosphere below the ozone number density peak (~25 km altitude), and while UARS MLS may be extended down to 100 hPa in ozone profile measurements, this limits maps of SCO to mostly tropical and subtropical latitudes. An important issue for the TOR method involving independent satellite instruments is interinstrument calibration which may seriously impact an accurate determination of TCO. Such calibration [*Chandra et al.*, 2003] can be obtained at locations where OMI can directly measure SCO using the Convective Cloud Differential (CCD) method [*Ziemke et al.*, 1998]. A main advantage of the new Aura MLS and OMI measurements is that near-global maps of calibrated TCO can be obtained on a daily basis which was not possible with previous satellite measurements.

[3] The OMI and MLS instruments on board the Aura spacecraft platform [*Schoeberl et al.*, 2004] have been providing global measurements of total and stratospheric column ozone soon after the launch of Aura on 15 July 2004 (Aura webpage: http://aura.gsfc.nasa.gov/). This has enabled near global measurements of TCO on almost a day-to-day basis from late August 2004 to present. The continuous global nature of the measurements allow the data to be compared with global models of tropospheric ozone in more detail than in previous studies. The previous studies were generally limited to tropical and subtropical latitudes [*Martin et al.*, 2000, 2002; *Peters et al.*, 2002; *Chandra et al.*, 2002;

[1]Goddard Earth Sciences and Technology, University of Maryland Baltimore County, Baltimore, Maryland, USA.
[2]Also at NASA Goddard Space Flight Center, Greenbelt, Maryland, USA.
[3]NASA Jet Propulsion Laboratory, Pasadena, California, USA.
[4]NASA Goddard Space Flight Center, Greenbelt, Maryland, USA.
[5]Royal Netherlands Meteorological Institute, De Bilt, Netherlands.

0148-0227/06/2006JD007089$09.00

Valks et al., 2003] and in some cases to higher latitudes in summer months [*Chandra et al.*, 2003, 2004]. Recently, *Liu et al.* [2006] have used the Goddard Earth Observing System Chemistry and transport (GEOS-CHEM) model to study global changes in tropospheric ozone based on Global Ozone Monitoring Experiment (GOME) measurements.

[4] The purpose of this paper is (1) to characterize the important basic features of the OMI/MLS TCO data set and (2) to analyze them in the context of a global transport model. The global model used in this study is the Global Modeling Initiative's (GMI) Combined Stratosphere-Troposphere Chemical Transport Model (COMBO CTM). The following sections begin with a description of the data followed by validation of the measurements (sections 2 and 3), monthly maps of tropospheric ozone from OMI/MLS (section 4), a description of the GMI COMBO CTM utilized in this study (section 5), comparisons between the model and OMI/MLS TCO (section 6), daily maps of OMI/MLS tropospheric ozone (section 7), and a summary (section 8).

2. Overview of Data

[5] MLS and OMI are two out of a total of four instruments on board the Aura spacecraft which is flown in a sun-synchronous polar orbit at 705 km altitude with a 98.2° inclination. The spacecraft has an equatorial crossing time of 1:45 pm (ascending node) with around 98.8 min per orbit (14.6 orbits per day on average).

[6] OMI is a nadir-scanning instrument that at visible (350–500 nm) and UV wavelength channels (UV-1: 270–314 nm; UV-2: 306–380 nm) detects backscattered solar radiance to measure column ozone with near global coverage (aside from polar night latitudes) over the Earth with a resolution of 13 km × 24 km at nadir. Aside from ozone, OMI can also determine cloud-top pressure, aerosols and aerosol parameters, NO_2, SO_2, and other trace constituents in the troposphere and stratosphere [*Levelt et al.*, 2006b]. Total ozone from OMI is derived from the TOMS version 8 algorithm. A description of this algorithm may be obtained from the TOMS V8 CD DVD ROM, or from the OMI Algorithm Theoretical Basis Document (ATBD) (from the Webpage http://toms.gsfc.nasa.gov/version8/v8toms_atbd.pdf).

[7] The MLS instrument is a thermal-emission microwave limb sounder that measures vertical profiles of mesospheric, stratospheric, and upper tropospheric temperature, ozone and other constituents from limb scans ahead of the Aura satellite. The MLS profile measurements are taken about 7 min before OMI views the same location during ascending (daytime) orbital tracks. These are referred as "collocated" measurements between OMI and MLS. MLS also measures ozone and other atmospheric constituents for descending nighttime orbits that on a given day can be up to ±12 hours different in time from OMI measurements. With combined ascending and descending nodes MLS makes around 3500 vertical profile measurements over the Earth per day. This study includes only the ascending orbit colocated data from MLS for deriving SCO. Details regarding the instrument including spectrometers, spectral channels, calibration, and other topics are discussed by *Waters et al.* [2006] and in related papers in the same journal. *Froidevaux et al.* [2006] provide early validation results on the Aura MLS version 1.5 measurements of ozone and other constituents.

[8] More than a year of Aura OMI and MLS ozone data have been archived as level 2 (L2, orbit/swath) and level 3 (L3, gridded) data beginning in August 2004. The OMI L3 and MLS L2 data are used to produce maps of SCO and TCO from daily to monthly means. All OMI/MLS SCO and TCO maps were first determined daily and then averaged temporally. In addition to L3 OMI measurements, OMI L2 footprint data were employed for deriving SCO and TCO from the CCD method. Both OMI and MLS measurements were screened via their L2 data quality flags. For MLS there are two data quality flags and a profile precision number for screening data; the retrieval errors can include several factors including problems associated with optically thick clouds in the troposphere which may affect retrieved ozone profiles. For OMI the version 8 algorithm includes an error flag for screening out scenes for high solar zenith angle (>84°), surface glint, SO_2 contamination, and several other factors. All OMI L3 total ozone data in this study were further screened for cloudy scenes by rejecting ozone measurements where OMI L3 reflectivity is greater than 0.3. This number was subjectively chosen after evaluation of critical values from 0.1 (too much data screened out) to 0.5 (too much cloud-related uncertainty in TCO, ~5+ DU in some measurements). The uncertainty in local TCO measurements from transient clouds using the 0.3 reflectivity criterion is ~2 DU. For calculating TCO and SCO it is necessary to have a measurement of tropopause pressure. For all evaluations of TCO and SCO in this study, tropopause pressure was determined from NCEP analyses using the 2 K km^{-1} thermal vertical gradient criterion of the World Meteorological Organization (WMO) [e.g., *Logan*, 1999, and references therein].

[9] The MLS ozone profile measurements were interpolated to the existing NCEP tropopause pressure to derive SCO. Measurements of MLS SCO (in Dobson Units, DU; 1 DU = 2.69×10^{16} molecules cm^{-2}) were determined by a standard method of pressure integration of ozone volume mixing ratio [e.g., *Ziemke et al.*, 2001, and references therein]: $SCO = 0.79 \int_{0.46hPa}^{Ptropopause} XdP$, where X is ozone volume mixing ratio in units ppbv and P is pressure in units hPa. The recommended range for useful scientific analysis of MLS v1.5 ozone profile data is 0.46–215 hPa [*Froidevaux et al.*, 2006]. MLS SCO data were binned to 1° latitude × 1.25° longitude to be compatible with OMI L3 gridded total ozone data. Tropopause pressures from NCEP analyses were rebinned to this same resolution from a coarser 2.5° × 2.5° gridding using 2D horizontal linear interpolation. It is noted for MLS limb measurements that the horizontal optical path is about 300 km which is larger than the horizontal size of OMI L3 gridded data, but is comparable to the size of original NCEP gridded measurements. We have used a two-step spatial interpolation of SCO from MLS along-track to derive 1° latitude × 1.25° longitude SCO maps similar to OMI L3 total column ozone. The interpolation for SCO includes first a moving 2D (latitude/longitude) Gaussian window along orbit to fill in intermittent gaps along-track for MLS SCO, followed

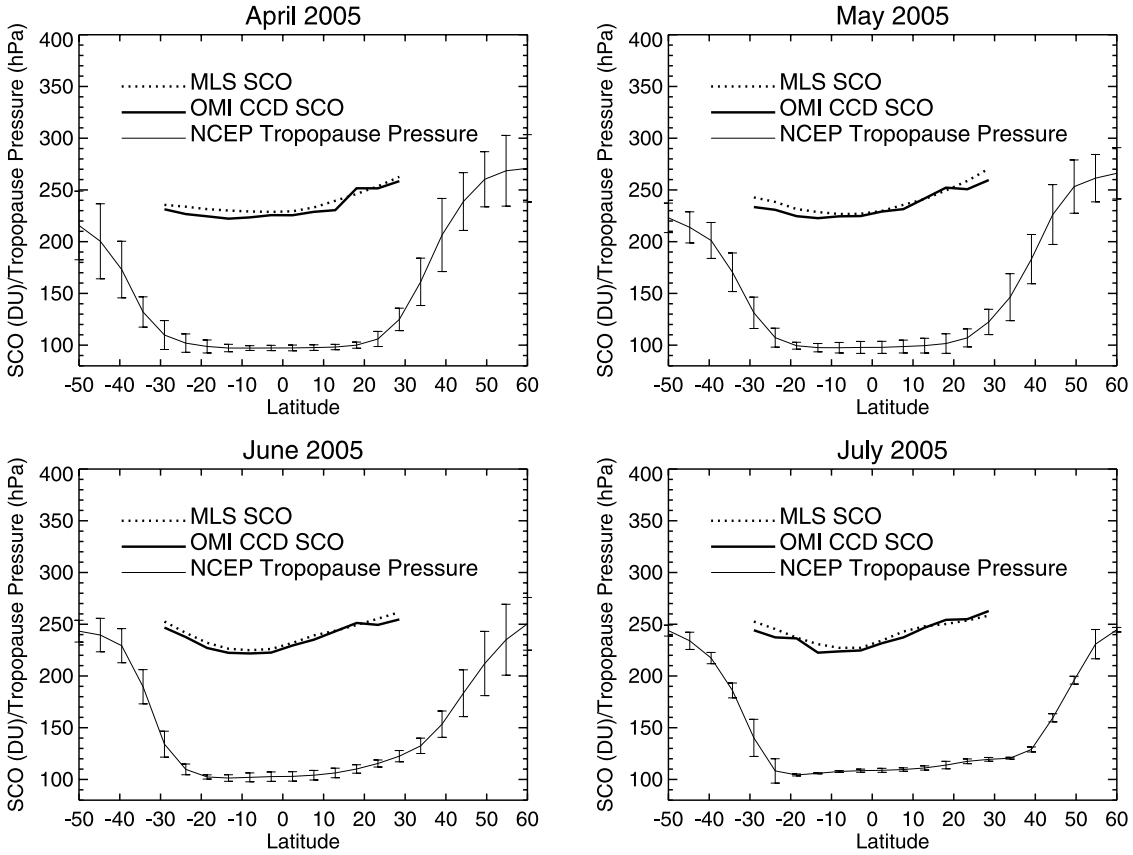

Figure 1. Four consecutive monthly averages of OMI CCD SCO (dark solid curves) and MLS ascending orbit SCO (dotted curves) averaged over the Pacific (120°W to 120°E). Also shown is NCEP tropopause pressure (bottom curves) averaged over the Pacific. Tropopause pressure for each month also shows $\pm 2\sigma$ values evaluated from the daily measurements. The numbers for SCO (DU) on the vertical axes also apply to NCEP tropopause pressure (hPa).

secondly by a linear interpolation along longitude between existing MLS SCO data.

3. Validation of OMI/MLS Tropospheric and Stratospheric Ozone Measurements

[10] *Froidevaux et al.* [2006] show an early validation analysis of the MLS ozone profile measurements. That study, along with similar analyses by others (D. Cunnold, personal communication, 2006) indicates that MLS tends to overestimate ozone in the lower stratosphere by several percent. The MLS validation efforts have compared ozone profile measurements with similar profile data from other satellite instruments including Stratospheric Aerosol and Gas Experiment (SAGE) II, Halogen Occultation Experiment (HALOE), Polar Ozone and Aerosol Measurement (POAM) III, and Atmospheric Chemistry Experiment (ACE). The MLS column ozone amounts evaluated for 0.46–215 hPa tend to be within about 1% of column amounts calculated from SAGE II.

[11] OMI total ozone measurements have been validated extensively by comparison with both ground-based Brewer and Dobson data, and also Earth Probe (EP) TOMS and Solar Backscatter Ultraviolet (SBUV) measurements from various National Oceanic and Atmospheric Administration (NOAA) satellites (G. Labow, personal communication, 2006). Comparisons between OMI and Dobson total ozone indicates that OMI is around 0.5% higher than the Dobson measurements. Measurements of total ozone from OMI and NOAA 16 are within 1% of each other for latitudes 60°S to 60°N. The validation of OMI/MLS tropospheric ozone includes comparisons with ozonesondes in the tropics and extratropics. The validation also entails comparisons between MLS SCO and SCO determined from the Convective Cloud Differential (CCD) method [*Ziemke et al.*, 1998; *Chandra et al.*, 2003].

3.1. Validation of MLS Stratospheric Ozone

[12] The efforts for validating OMI/MLS tropospheric and stratospheric ozone begin first by comparing MLS SCO with OMI CCD SCO. The CCD measurements of SCO from TOMS instruments have been extensively tested in previous studies. Recently *Ziemke et al.* [2005] found excellent agreement ($\sim$1–3 DU offsets, $\sim$4–5 DU RMS differences) in the tropics between SAGE II and TOMS CCD SCO for the 1984–2003 time record. In an effort to minimize potential errors in these comparisons caused by large dynamical variabilities in SCO (associated with large fluctuations in the tropopause), the analyses were limited to regions primarily equatorward of the subtropical wind jets.

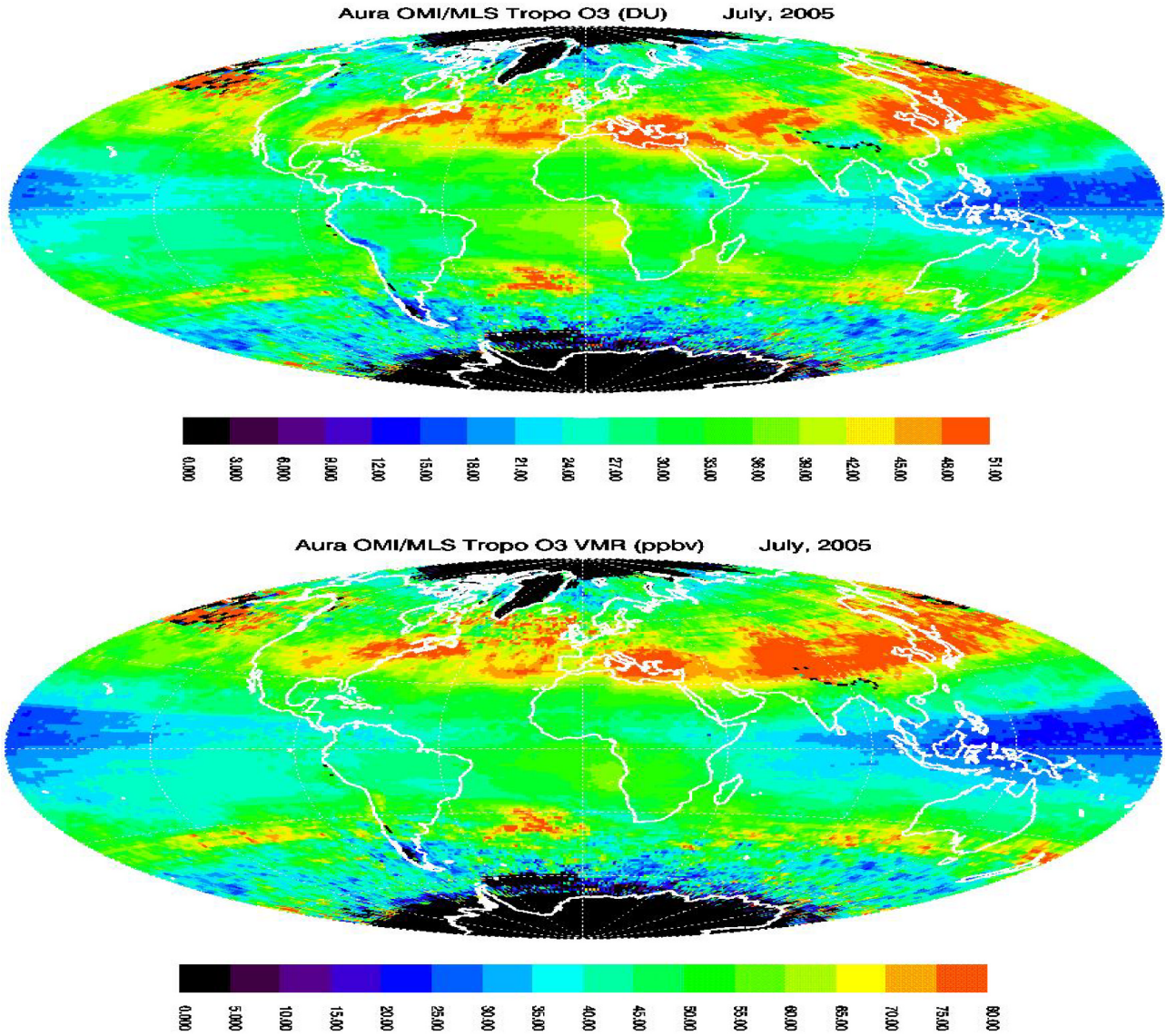

Figure 2. (top) OMI/MLS TCO (in DU) and (bottom) tropospheric ozone mean VMR (in ppbv) for July 2005. The color scale increments have different values for the two plots; on average, 30 DU in TCO corresponds to around 50 ppbv in VMR. The color bar for TCO (Figure 2, top) goes from zero to 51 DU in steps of 3 DU. The color bar for VMR (Figure 2, bottom) goes from zero to 80 ppbv in steps of 5 ppbv.

This was done by restricting latitudes in the comparisons to ±30°. Measurements from the CCD method are limited to regions with a sufficient number of convective clouds to estimate SCO. For this study the CCD measurements were restricted to the Pacific region. Both OMI CCD and MLS measurements of SCO are averaged over the Pacific (120°W to 120°E about the dateline) for the comparisons.

[13] Figure 1 shows four consecutive monthly averages of OMI CCD SCO (dark solid curves) and MLS SCO (dotted curves) over the Pacific. Also shown in Figure 1 are Pacific averages of NCEP tropopause pressure (bottom solid curves). To illustrate the variability of tropopause pressure, $\pm 2\sigma$ values (vertical bars) are included, where σ represents the standard RMS value evaluated from daily Pacific-mean measurements for each month. In Figure 1 tropopause pressure in any month does not deviate substantially from 100 hPa in the latitude range 30°S to 30°N; this suggests that the comparisons between OMI and MLS SCO are made for a predominantly tropical air mass condition.

[14] An important application of the CCD method is that the SCO measurements can be used to cross-calibrate MLS SCO to that of OMI prior to deriving TCO [*Chandra et al.*, 2003]. A mean instrument measurement offset in SCO was determined to be 3.8 DU (OMI less than MLS) from the data in Figure 1. (The calculated RMS value for this mean offset number is 1.5 DU.) This adjustment was applied to MLS SCO in this study for deriving calibrated measurements of TCO from OMI and MLS residual difference. For the first year of OMI and MLS SCO measurements the offset present is relatively small; however, this may change in the future.

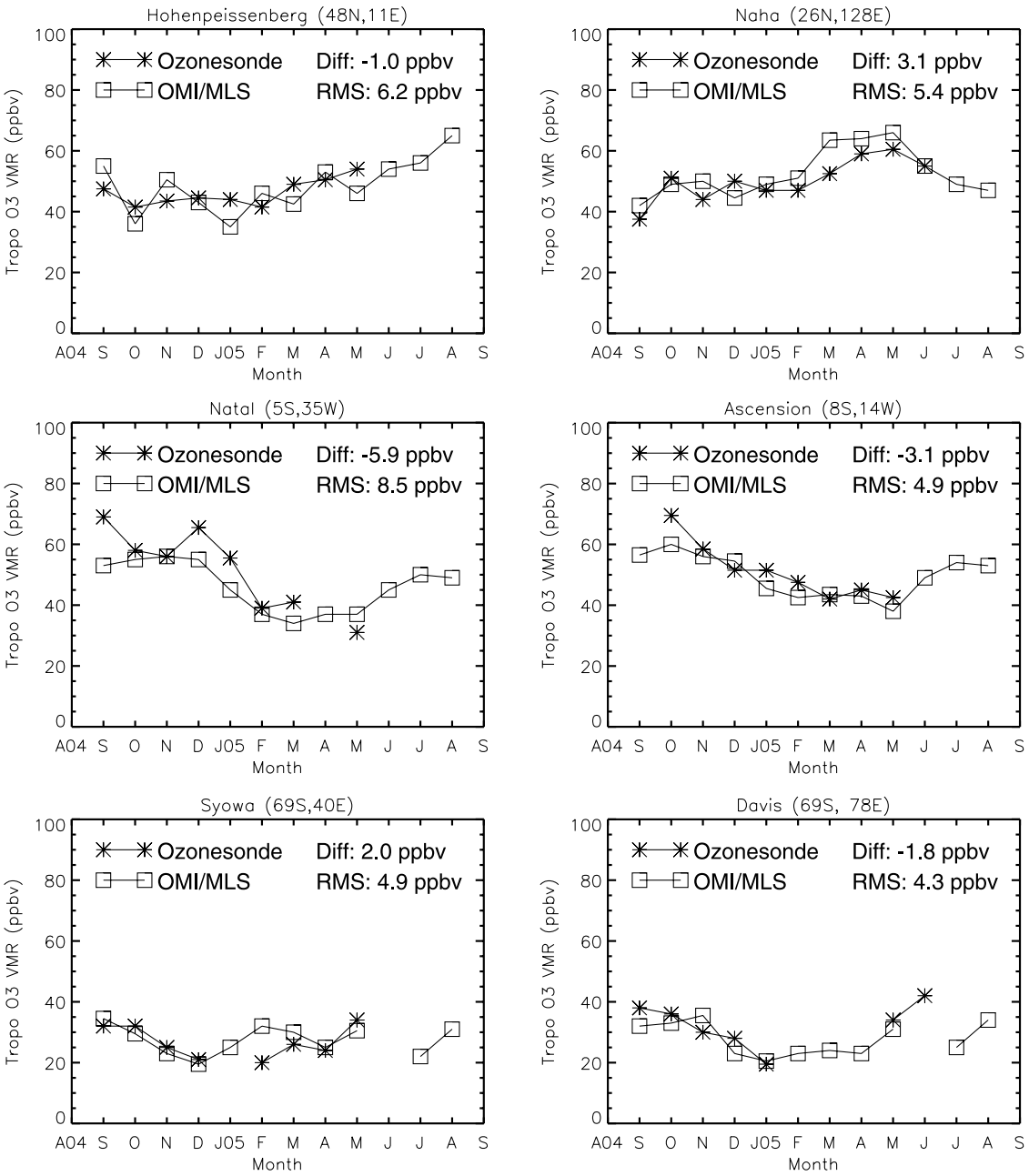

Figure 3. Time series comparisons of monthly averaged tropospheric ozone VMR (in ppbv) from OMI/MLS (boxes) and ozonesondes (stars) for September 2004 to August 2005. The ozonesondes include extratropical WOUDC and tropical SHADOZ measurements. Included for each station are the mean difference (OMI/MLS minus ozonesonde) and the standard RMS of this difference.

3.2. Validation of OMI/MLS Tropospheric Ozone

[15] OMI/MLS tropospheric ozone was compared with Southern Hemisphere ADditional OZonesondes (SHADOZ) [*Thompson et al.*, 2003] in the tropics and World Ozone and Ultraviolet radiation Data Center (WOUDC) outside the tropics. There are systematic problems when comparing ozonesondes with OMI/MLS satellite measurements, two of them being that ozonesondes are "point" measurements compared to OMI/MLS (which is an average over a large geographical region), and ozonesondes are sparse measurements ($\sim$1–4 profiles per month) which is especially troublesome in dynamically active regions. For tropical SHADOZ measurements there is only small variability of the tropopause pressure year-round ($\pm$10 hPa) with mean values around 100 hPa. However, comparing OMI/MLS tropospheric ozone with sparse ozonesonde measurements outside the tropics is difficult in the subtropics/midlatitudes which are associated with large day-to-day variability of tropopause height. This produces additional noise in the comparisons of sparse data since the calculation of TCO relies directly on tropopause pressure. Even if the ozone concentration (i.e., mixing ratio) in the troposphere

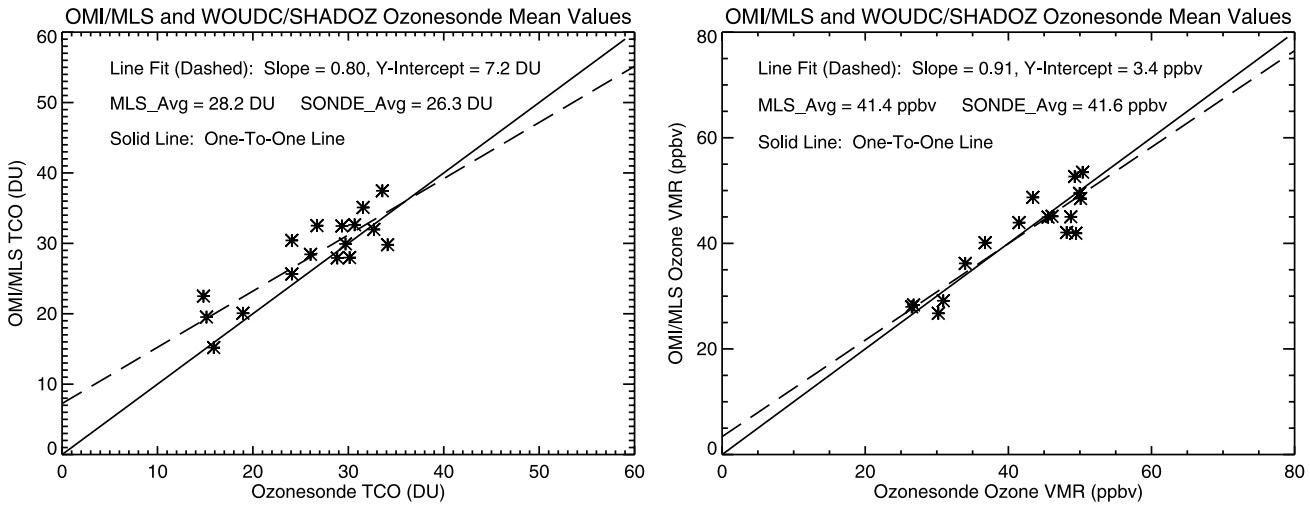

Figure 4. (left) OMI/MLS versus ozonesonde TCO (in DU) for several WOUDC and SHADOZ sites averaged for September 2004 to August 2005. (right) Same as Figure 4 (left) but for mean ozone VMR (in ppbv). Also shown in this figure are regression line fits to the data (dashed lines), and the one-to-one line (solid).

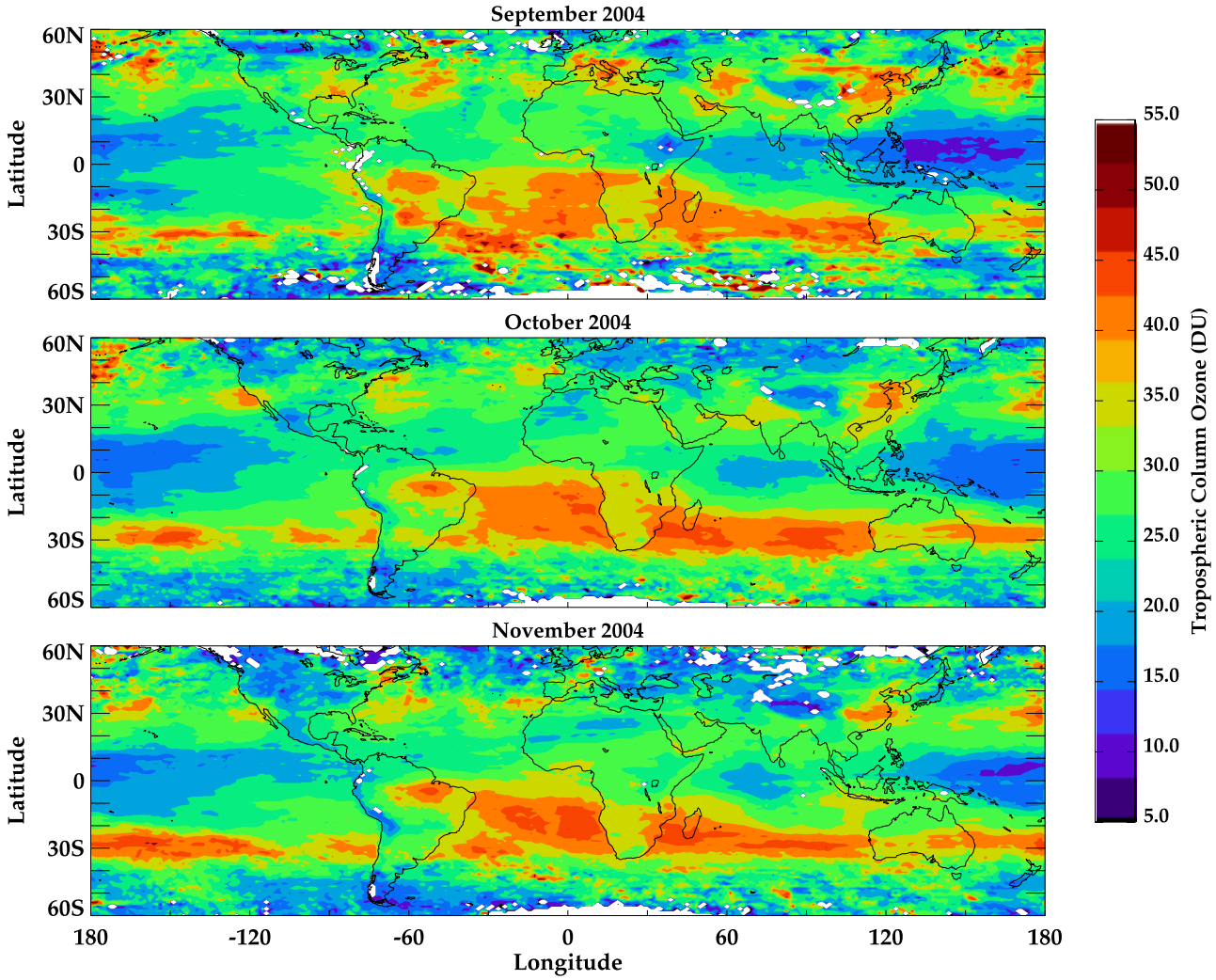

Figure 5a. Monthly averaged OMI/MLS TCO (in DU) for September–November 2004.

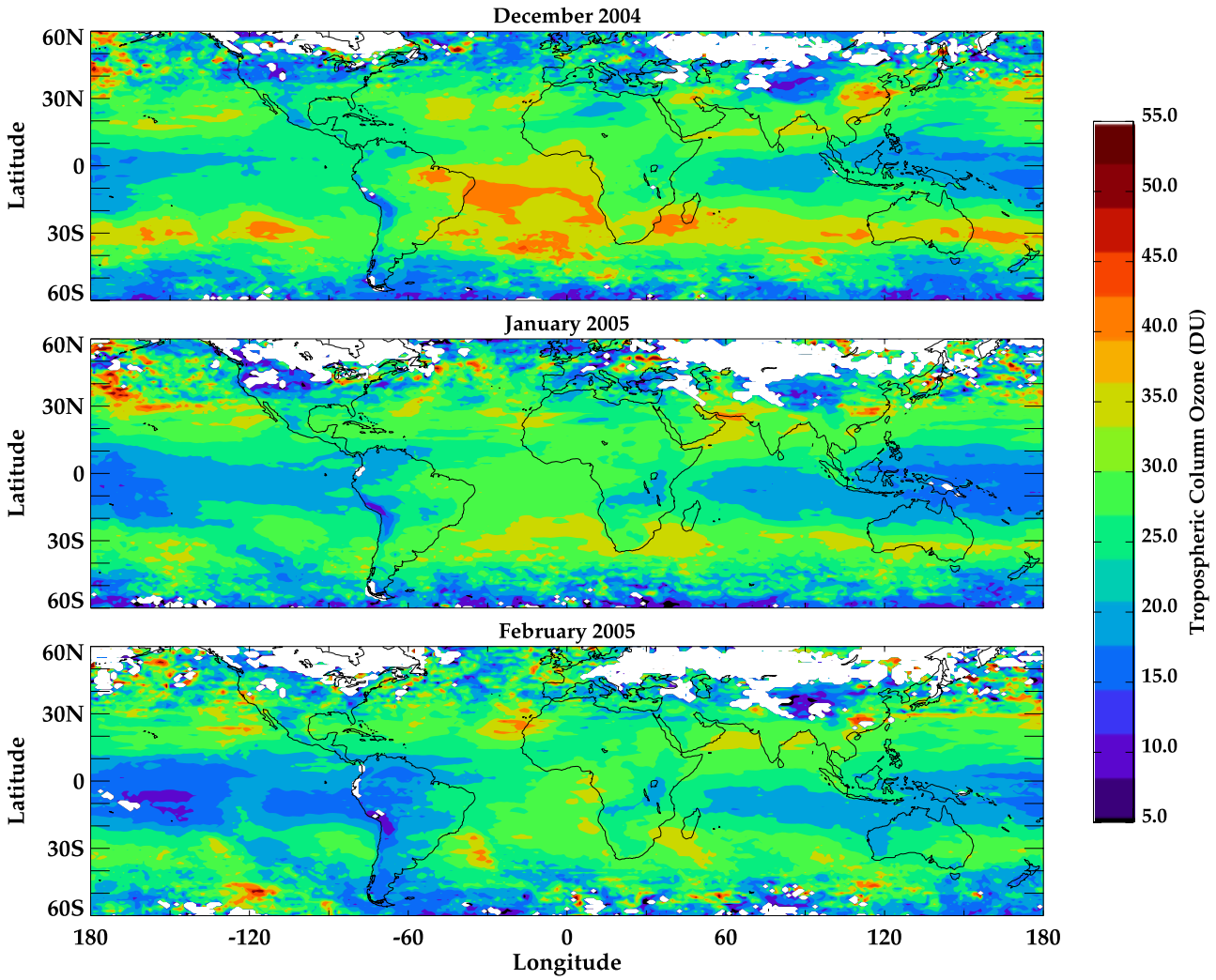

Figure 5b. Same as Figure 5a but for December 2004 to February 2005.

between days does not change, TCO will increase/decrease from a decrease/increase in tropopause pressure.

[16] A different interpretation of tropospheric ozone may be utilized to reduce these noise problems for validation with WOUDC ozonesondes outside the tropics. The measurement of tropospheric ozone may also be inferred by calculating a pressure-averaged ozone volume mixing ratio (VMR): VMR = 1.27 × TCO/($P_{Terrain}$ − $P_{Tropopause}$), where VMR is in parts per million by volume (ppmv), TCO is in DU, and $P_{Terrain}$ and $P_{Tropopause}$ are in hPa [e.g., *Ziemke et al.*, 2001, and references therein].

[17] Figure 2 shows color contour diagrams of OMI/MLS TCO (Figure 2, top) and ozone mean VMR (Figure 2, bottom) averaged for July 2005. Although the recommended range for MLS ozone profile measurements is 0.46–215 hPa, our evaluation of the data suggests that this range can be extended to 316 hPa (next higher pressure level beyond 215 hPa retrieved by MLS) for determining SCO. Extending MLS data to the maximum value of 316 hPa for measuring SCO provides nearly global coverage, and for the remainder of this study the upper bound of 316 hPa is implemented. SCO is determined by integrating MLS ozone from 0.46 hPa down to the NCEP tropopause (not to exceed 316 hPa).

[18] In general, TCO and ozone VMR in Figure 2 have similar spatial patterns on a monthly timescale except in regions where changes in tropopause pressure or terrain pressure are significant (such as the Himalayas and Andes). On average, 30 DU in TCO corresponds to about 50 ppbv in VMR. Because previous studies of tropospheric ozone from satellite measurements have evaluated TCO rather than VMR, this study including figures involves mostly TCO. There are many features present in Figure 2 including ozone enhancements over the eastern U.S., Asia, Mediterranean, and over oceans in the Northern Hemisphere. These and other features over the 12-month record will be discussed in later sections of this paper.

[19] Figure 3 shows time series comparisons for September 2004 to August 2005 of monthly averaged tropospheric ozone VMR from OMI/MLS (boxes) and ozonesondes (stars). The ozonesonde data are generally sparse with about 3–4 measurements per month with some months having only 1 or 2 measurements. VMR at Hohenpeissenberg (48°N) is largest around summer months while for Naha

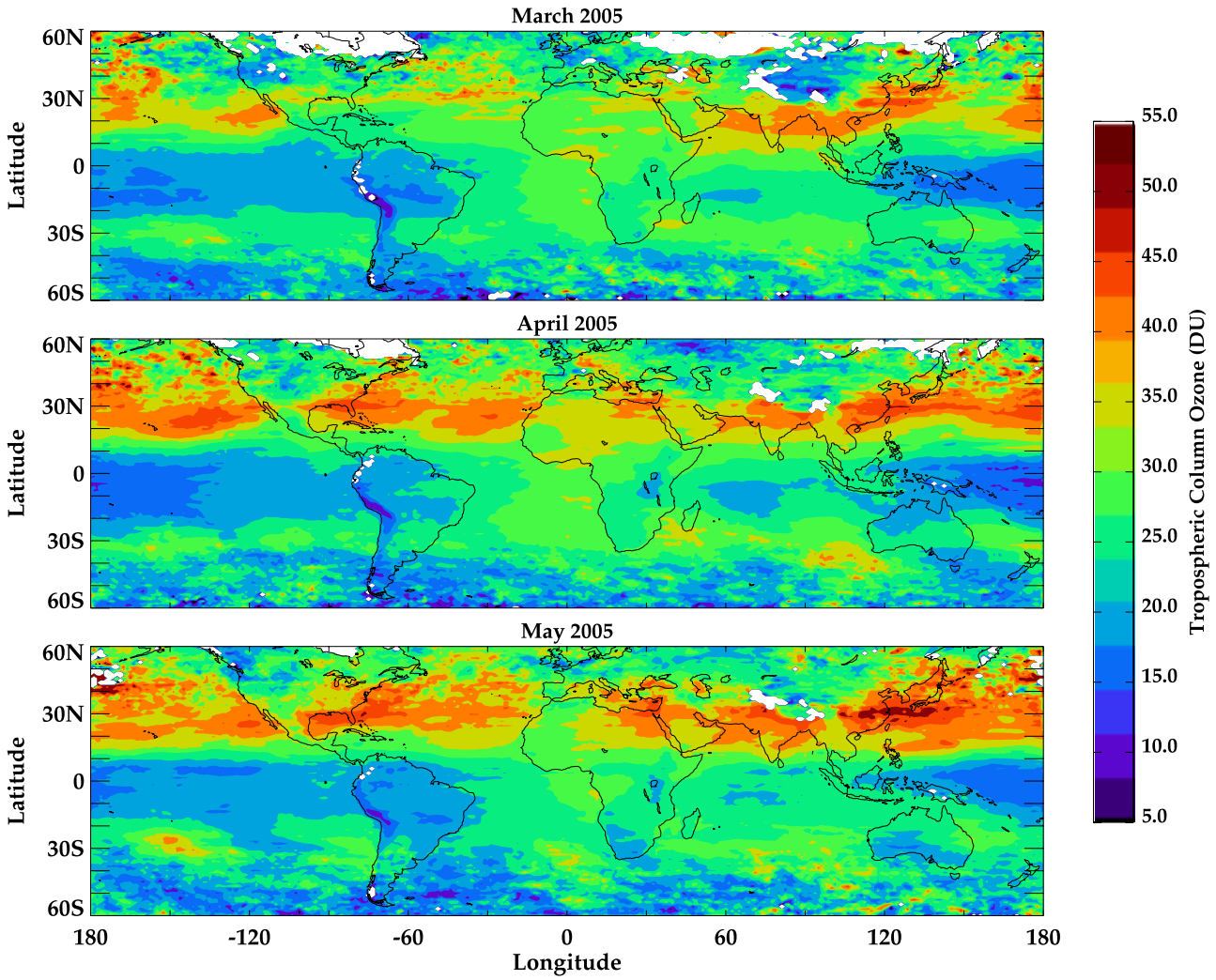

Figure 5c. Same as Figure 5a but for March 2005 to May 2005.

at 26°N in the western Pacific largest ozone occurs in late spring. For tropical Atlantic stations Natal and Ascension Island, ozone appears lowest around March–May and largest in August–November months. The differences in ozone seasonal cycles between tropical and extratropical stations in the Northern Hemisphere are caused by differing dominant sources of tropospheric ozone including stratosphere-troposphere exchange (STE) and industrial pollution in the extratropics, and biomass burning in the tropics.

[20] The last two frames in Figure 3 are Antarctic stations, Syowa and Davis at 69°S. VMR for these stations is substantially lower than the other stations and shows amounts down to 20 ppbv in austral summer and autumn. These low ozone amounts are comparable to values found in the generally pristine tropical Pacific region. The low VMR in the southern high latitudes is a manifestation of low levels of ozone-producing sources in the troposphere and small influence from STE [e.g., *de Laat et al.*, 2005, Figure 2]. The average station value for both ozonesonde VMR and OMI/MLS VMR in Figure 3 is 41.8 ppbv, while the average RMS difference of monthly means is 7.2 ppbv.

[21] Ozone VMR may provide a less noisy validation test when compared to TCO for sparse measurements such as ozonesondes, especially in the dynamically active extra-tropics where the tropopause may fluctuate substantially. This is illustrated in Figure 4 which compares TCO from OMI/MLS versus ozonesondes (Figure 4, left) and ozone VMR from OMI/MLS versus ozonesondes (Figure 4, right). All data were averaged over the full year of existing measurements and includes both WOUDC and SHADOZ ozonesondes. The WOUDC data in Figure 4 also includes several other midlatitude ground stations not shown in Figure 3. Although the mean offset difference for TCO (Figure 4, left) is only about 2 DU, there is obvious scatter present and the regression line deviates measurably from the one-to-one line which is shown as solid in Figure 4. VMR (Figure 4, right) in contrast exhibits less scatter and a regression line closer to the one-to-one line. Mean values of VMR for OMI/MLS and ozonesondes are nearly equal at ~41 ppbv. The four lowest values of VMR and TCO in Figure 4 coincide with two WOUDC Antarctic stations (i.e., the two Antarctic stations plotted in Figure 3) and two SHADOZ tropical stations. The higher values of TCO and VMR in Figure 4 originate from primarily Northern Hemisphere midlatitude stations. It is noted that there are other sources of scatter in Figure 4 including simple noise in

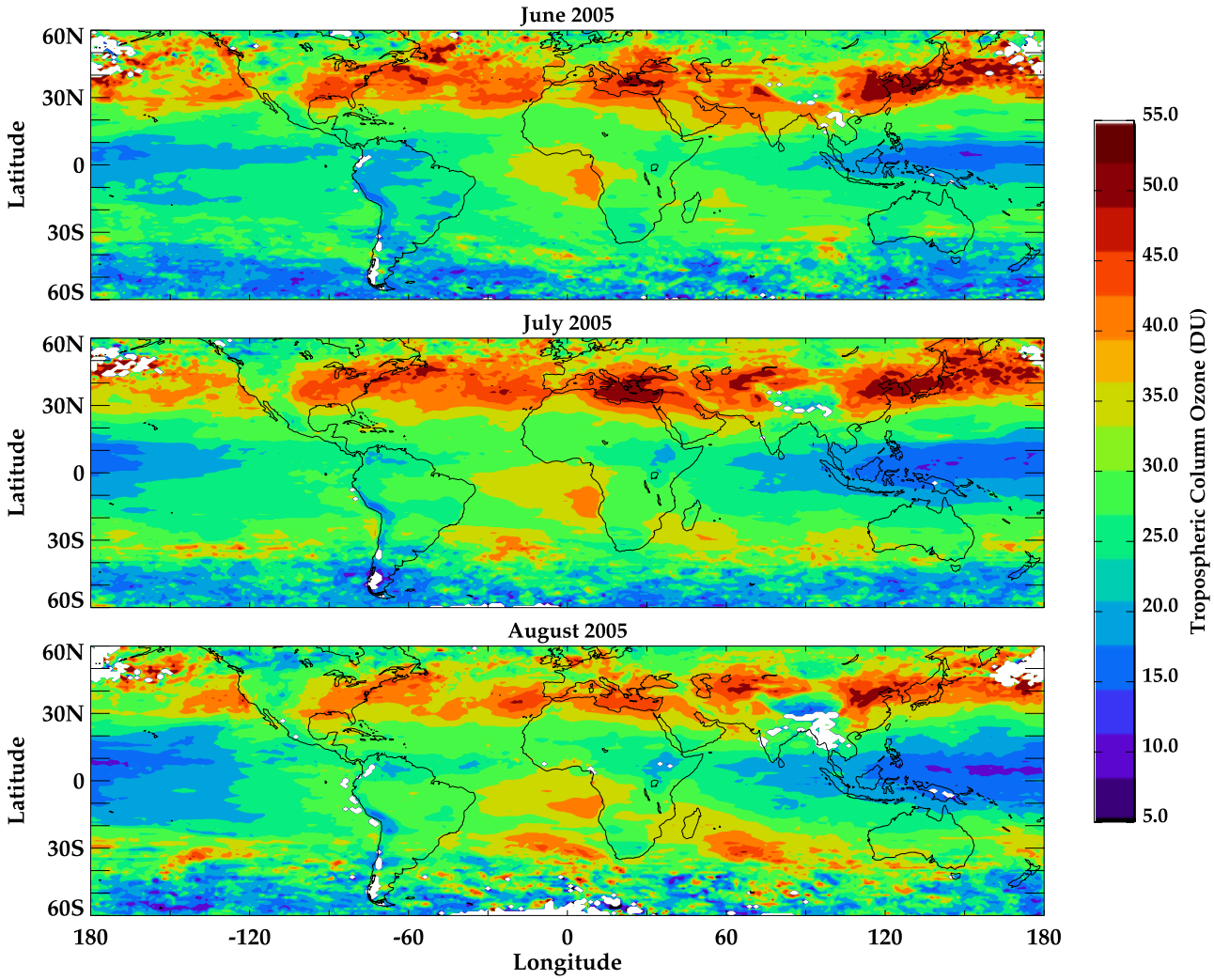

Figure 5d. Same as Figure 5a but for June 2005 to August 2005.

ozone and tropopause pressures, and also the basic nature of ozonesondes as being "point" measurements compared to OMI/MLS which is an average measurement over a generally broad geographical region (which smoothes out terrain variation effects). Using ozonesondes as reference, RMS uncertainties in local measurements of TCO from OMI/MLS are about 5 DU (or about 8 ppbv in VMR).

[22] Two conclusions from Figure 4 are that (1) neither OMI/MLS TCO nor mean VMR for the first year of Aura measurements exhibit substantial offset differences relative to ozonesondes and (2) for validation purposes involving midlatitudes with sparse ozonesonde data it may be better to compare ozone VMR rather than TCO because of added noise generated from tropopause height fluctuations.

4. Monthly Maps of Tropospheric Ozone From OMI/MLS

[23] Our first evaluation of tropospheric ozone from OMI and MLS is to examine one complete year of monthly means for September 2004 to August 2005 and characterize basic properties including annual variability and regional patterns. Figures 5a–5d shows four panels of OMI/MLS monthly mean TCO evaluated for September–November, December–February, March–May, and June–August. The number of days of OMI/MLS measurements per month for September 2004 to August 2005 were 12, 27, 18, 25, 20, 17, 31, 28, 23, 20, 27, and 16, respectively (missing days are due primarily to profile retrieval difficulties with MLS).

[24] For September–November (Figure 5a) high values of TCO lie in the Southern Hemisphere along a zonal band around 30–40°S. They are similar to high TCO values at midlatitudes in the Northern Hemisphere in summer and spring months (Figures 5c and 5d). These seasonal enhancements are of dynamical origin caused by STE [e.g., *Lelieveld and Dentener*, 2000; *de Laat et al.*, 2005, and references therein]. Figure 5a also shows a well-known feature of the tropical troposphere, i.e., an enhancement in TCO over the Atlantic Ocean between South America and Africa, and decrease over a wide region in the Pacific. This feature is often referred to as a wave-one feature of the tropical troposphere and is robust in September, October, and November months. The origin of the wave one in TCO is a manifestation of several contributing factors including

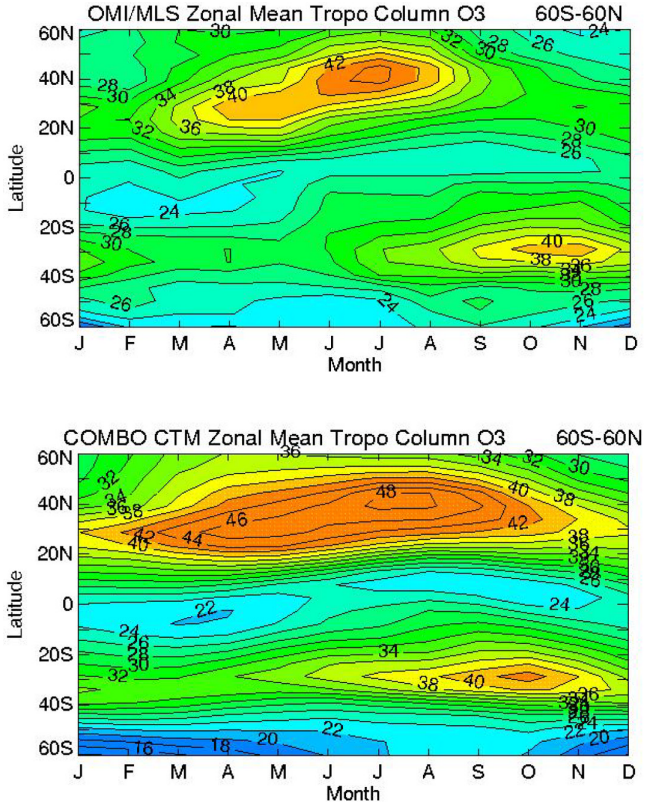

Figure 6. Monthly zonal mean TCO (in DU) from (top) OMI/MLS and (bottom) COMBO CTM. The annual cycles from the model were averaged over 5 years. The annual cycles from OMI/MLS represent 1 year of measurements from September 2004 to August 2005.

biomass burning and lightning in both Africa and South America, and enhanced convection in the Pacific region coupled with the large scale Walker Circulation. The south Atlantic enhancement of tropospheric ozone and its dynamical/photochemical sources has been studied extensively in recent years using global models of transport and chemistry [e.g., *Wang et al.*, 1998; *Lelieveld and Dentener*, 2000; *Marufu et al.*, 2000; *Moxim and Levy*, 2000; *Singh et al.*, 2000; *Martin et al.*, 2002; *Chandra et al.*, 2002, 2003; *Edwards et al.*, 2003]. In December–February (Figure 5b) a transition occurs whereby the high ozone present in the Southern Hemisphere in the previous three months is substantially reduced. January and February show the lowest levels of globally averaged ozone (averaged between 60°S and 60°N) in the troposphere for the year of OMI/MLS data analyzed in this study. January and February months also have the most hemispheric symmetry in TCO of all 12 months. The symmetry in these months is explained in part by a seasonal minimum in biomass burning [e.g., *Duncan et al.*, 2003].

[25] For March–May (Figure 5c), TCO is enhanced in the northern subtropics and midlatitudes from STE, which is at an annual maximum in this zonal band. Photochemical production of ozone also becomes important in spring. TCO in the northern midlatitudes is as large over the Atlantic and Pacific Oceans as it is over industrial emission regions [*Chandra et al.*, 2004].

[26] For June–August most ozone lies in the northern subtropics and midlatitudes (Figure 5d). Global OMI/MLS TCO averaged between 60°S is 60°N is largest for June–August than other months of the year because of the photochemical production of ozone from both anthropogenic pollution and biogenic volatile organic compounds and NO_x. Large enhancements of ozone for June–August lie over eastern China and downwind across the Pacific Ocean to North America, and over the eastern U.S. and downwind across the Atlantic Ocean. There is also a local enhancement over the Mediterranean region. The modeling study by *Lelieveld et al.* [2002] described a Mediterranean enhancement of tropospheric ozone during summer months in their model as an accumulation "crossroads" effect.

5. Global Modeling Initiative Combined Stratosphere-Troposphere CTM

[27] The GMI has developed several interrelated CTMs, including a stratosphere-only, a troposphere-only, and a combined stratosphere/troposphere model, or COMBO CTM. The COMBO CTM is used in this study to simulate tropospheric ozone and compare with measurements from OMI/MLS. The COMBO CTM was developed from the initial stratosphere-only CTM described by *Rotman et al.* [2001]. Brief descriptions of this model are given by *Considine et al.* [2004, 2005]. As the version of the COMBO CTM used here is relatively new, evaluations of the model's performance with trace gas observations, including in the troposphere, are forthcoming. We discuss this issue further at the end of this section.

[28] The chemical mechanism in this model is obtained by combining tropospheric and stratospheric full mechanisms. The tropospheric mechanism includes a detailed description of O_3-NO_x-hydrocarbon chemistry [*Bey et al.*, 2001]. It has been updated with recent experimental data, such as the removal of $O(^1D)$ by several atmospheric molecules [*Dunlea and Ravishankara*, 2004]. Photolysis frequencies are computed using the Fast-JX radiative transfer algorithm, which combines the Fast-J tropospheric photolysis scheme described by *Wild et al.* [2000] with the Fast-J2 stratospheric photolysis scheme of *Bian and Prather* [2002] (M. Prather, personal communication, 2005). The scheme treats both Rayleigh scattering as well as Mie scattering by clouds and aerosols. The stratospheric chemistry mechanism is described by *Kinnison et al.* [2001] and *Douglass et al.* [2004]. A description of the Polar Stratospheric Cloud parameterization is provided by *Considine et al.* [2000]. The chemical mass balance equations are integrated using the SMVGEAR II algorithm [*Jacobson*, 1995].

[29] The trace gas emission inventories are presented by *Bey et al.* [2001] and *Duncan et al.* [2003] and represent rates typical of the mid-1990s. The lightning source is set to 5.0 Tg N/y and is horizontally distributed using monthly mean lightning emissions based on the locations and heights of deep convective clouds from the ISCCP cloud climatology [*Price et al.*, 1997]. Lightning flash rates used in constructing these monthly mean emissions are based on the cloud-top height parameterization of *Price and Rind* [1992]. The vertical distribution of the lightning NO_x is specified by the profiles derived from cloud-resolved con-

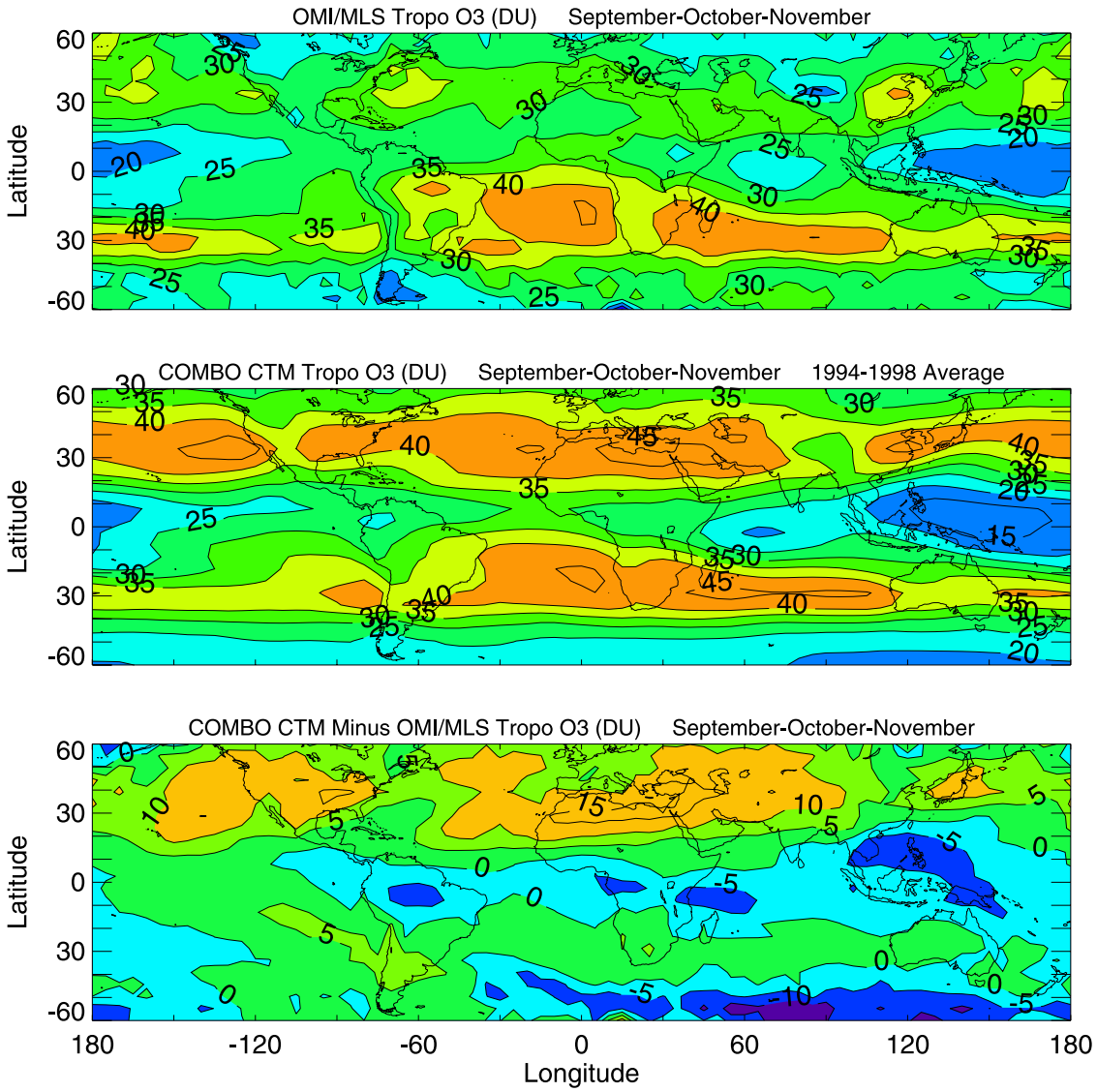

Figure 7a. Seasonal (3-month) averages of (top) OMI/MLS TCO, (middle) model TCO, and (bottom) CTM minus OMI/MLS difference for September–November. Seasonal mean TCO for the model were averaged over 5 years. For OMI/MLS, TCO represents seasonal averages from September 2004 to August 2005 measurements.

vection simulations of *Pickering et al.* [1998]. Mixing ratio boundary conditions are imposed for halogen source gases for conditions appropriate for 2001. The COMBO CTM simulates the radiative and heterogeneous chemical effects of sulfate, dust, sea-salt, organic carbon and black carbon aerosol on tropospheric photochemistry. The three-dimensional aerosol surface area distributions were obtained from the Goddard Chemistry Aerosol Radiation and Transport (GOCART) model [*Chin et al.*, 2002], taking into account swelling of aerosols in humid environments. The aerosol fields were coupled to the COMBO CTM as described by *Martin et al.* [2003].

[30] The COMBO CTM uses the advection scheme of *Lin and Rood* [1996]. Convective transport of species is taken from the MATCH model [*Rasch et al.*, 1997]. MATCH uses the following GEOS-4-AGCM meteorological fields [e.g., *Bloom et al.*, 2005] as input: cloud mass fluxes, entrainment and detrainment fluxes, and large-scale downwelling. Both shallow and deep convection are considered, following the algorithms of *Hack* [1994] and *Zhang and McFarlane* [1995]. The COMBO CTM uses the Harvard wet scavenging algorithm as described by *Liu et al.* [2001] and the dry deposition scheme as described by *Wang et al.* [1998], which follows the methodology of *Wesely et al.* [1985].

[31] Transport in the COMBO CTM is driven by 5 years [1994–1998] of meteorological fields from the Goddard Earth Observing System (GEOS), version 4, of the Goddard Modeling and Assimilation Office (GMAO) atmospheric global circulation model (AGCM). The GEOS-4-AGCM fields have been regridded to 42 vertical levels to 0.01 hPa and a horizontal resolution of 2° latitude × 2.5° longitude. The fields were generated using sea-surface temperatures (SSTs), representing 1994 to 1998. *Douglass et al.* [2003] show that the large-scale circulation, including STE, is realistic in a CTM driven by these fields. The COMBO CTM with GEOS-4-AGCM fields was used in a study by

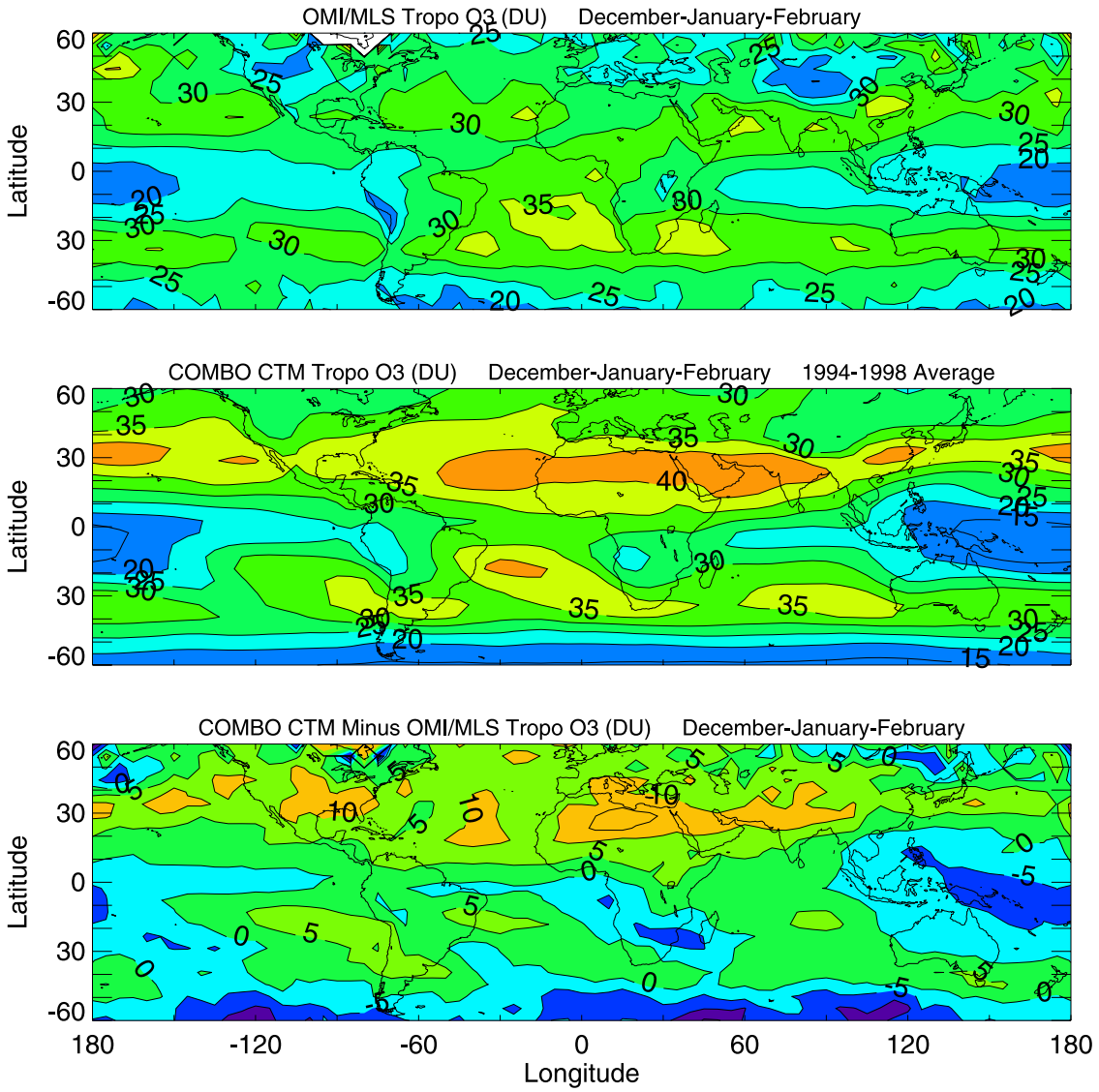

Figure 7b. Same as Figure 7a but for December–February.

Schoeberl et al. [2006], who identified the stratospheric "tape recorder" in carbon monoxide (CO), a seasonal oscillation in tropical lower stratospheric CO due to transport from the upper troposphere, in the Aura Microwave Limb Sounder (MLS) data. The seasonality and vertical extent of the CO tape recorder as simulated by the model compare well to the observations.

[32] The COMBO CTM with transport driven by the GEOS-4-AGCM fields overpredicts upper tropospheric ozone as compared to ozonesondes year-round in the Northern Hemisphere midlatitudes, especially in late winter/early spring and over the Middle East in summer (J. Logan, personal communication, 2005). Consequently, the model TCO is biased high compared to the OMI/MLS TCO in this zonal band, as shown in section 6. The source of the model's overprediction in late winter/early spring is likely due in part to overestimation of stratosphere-to-troposphere ozone flux, since STE is known to maximize in the Northern Hemisphere midlatitudes at that time.

[33] The tropospheric version of the GMI model participated in a recent model intercomparison study, IPCC/ACCENT. The model's budget of ozone fell within one standard deviation of the mean of 26 models [*Stevenson et al.*, 2006]. A comparison of the model's nitrogen dioxide concentrations with measurements from the GOME instrument shows that the model is biased low, a common problem for most of the models participating in the intercomparison [*van Noije et al.*, 2006]. For CO, the model is biased low generally everywhere as compared to MOPITT observations, except in the tropics in the first half of the year [*Shindell et al.*, 2006]. All participating models were biased low in the Northern Hemisphere extratropics, likely because of too low fossil fuel emissions used in the intercomparison.

6. Tropospheric Ozone Columns: OMI/MLS Versus GMI COMBO CTM

[34] In comparing the seasonal and zonal characteristics of TCO from OMI/MLS with the COMBO CTM, we are

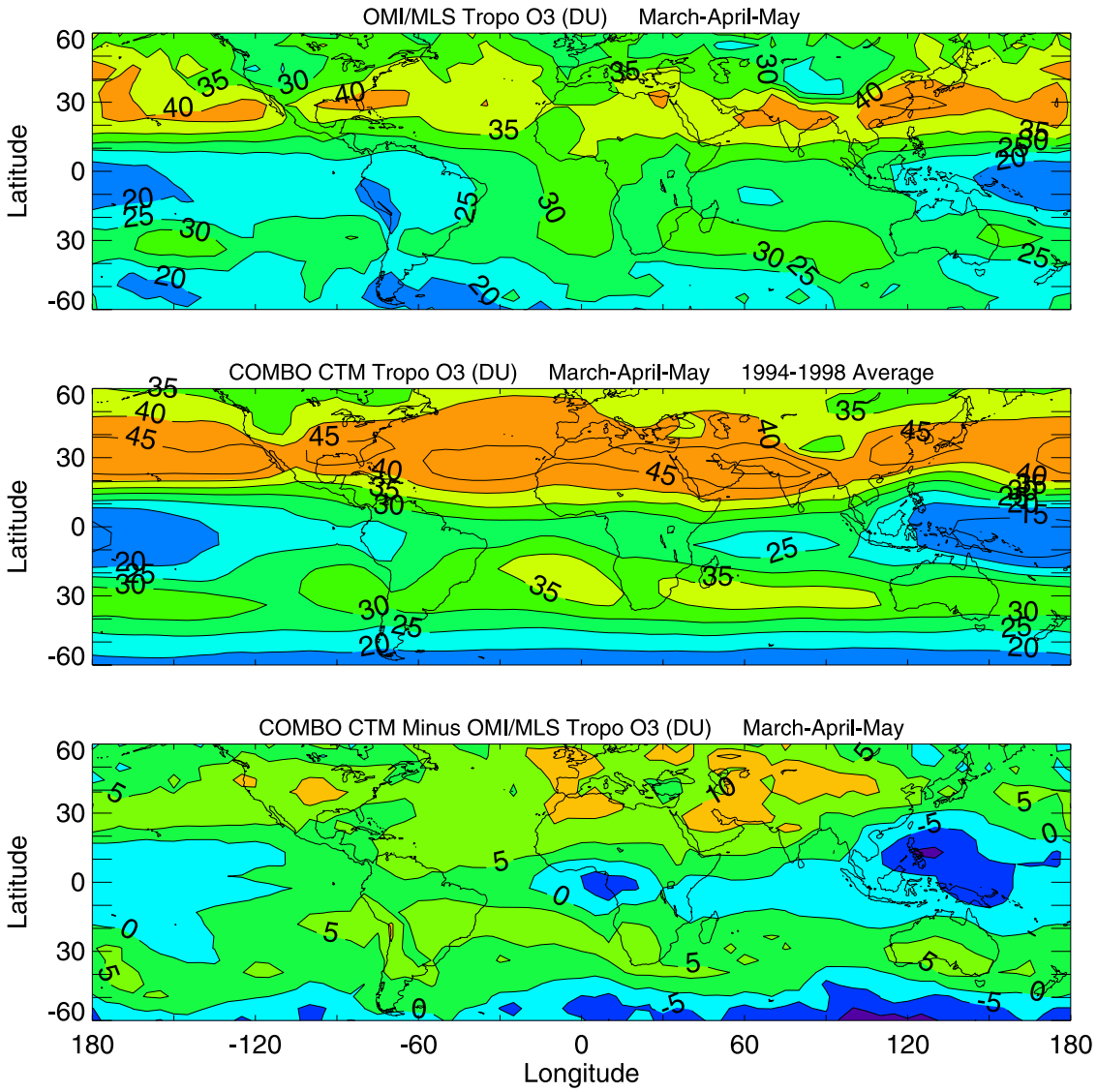

Figure 7c. Same as Figure 7a but for March–May.

constrained to use the model results transport driven by GCM fields forced by observed SSTs for 1994–1998. A model simulation with assimilated fields for 2004–2005 is not yet available. The evaluation of the modeled and observed TCO fields is therefore limited to comparing their broad features. Figure 6 compares the seasonal characteristics of zonal mean TCO from OMI/MLS (Figure 6, top) and the COMBO CTM (Figure 6, bottom). The OMI/MLS values are for September 2004 to August 2005 and model values are taken as a 5-year average. The year-to-year variability for any given month and grid point in the model is generally small (~1–3 DU), except in regions impacted by dynamical changes associated with the El Niño/Southern Oscillation phenomenon [*Chandra et al.*, 2002]. As seen in Figure 6, TCO from COMBO CTM and OMI/MLS TCO agree within a few DU and have similar basic features which include (1) a seasonal shift in maximum ozone in the Northern Hemisphere extending from tropical and subtropical latitudes in spring months to midlatitudes in summer, (2) smallest year-round ozone amounts in the tropics and also high southern latitudes, and (3) a large annual cycle in TCO in the Southern Hemisphere in the subtropics around 30°S with maximum values in September–November. (The September–November maximum dominates most southern latitudes from the tropics to 50–60°S.)

[35] Figures 7a–7d show seasonal averages (3-month averages) of OMI/MLS TCO (top), model TCO (middle), and their difference (bottom) for September–November, December–February, March–May, and June–August, respectively. As in Figure 6, the model TCO in Figure 7a–7d is presented as a 5-year mean.

[36] TCO fields for September–November (Figure 7a) for both model and OMI/MLS are similar in the Southern Hemisphere with largest values around 40–45 DU in the south Atlantic, and low ozone amounts ~20 DU over the tropical Pacific and high southern latitudes. The largest differences between OMI/MLS and model TCO lie in the Northern Hemisphere with OMI/MLS TCO around 5–10 DU smaller than model TCO. Differences of +10 DU lie in a band extending from Saudi Arabia westward across

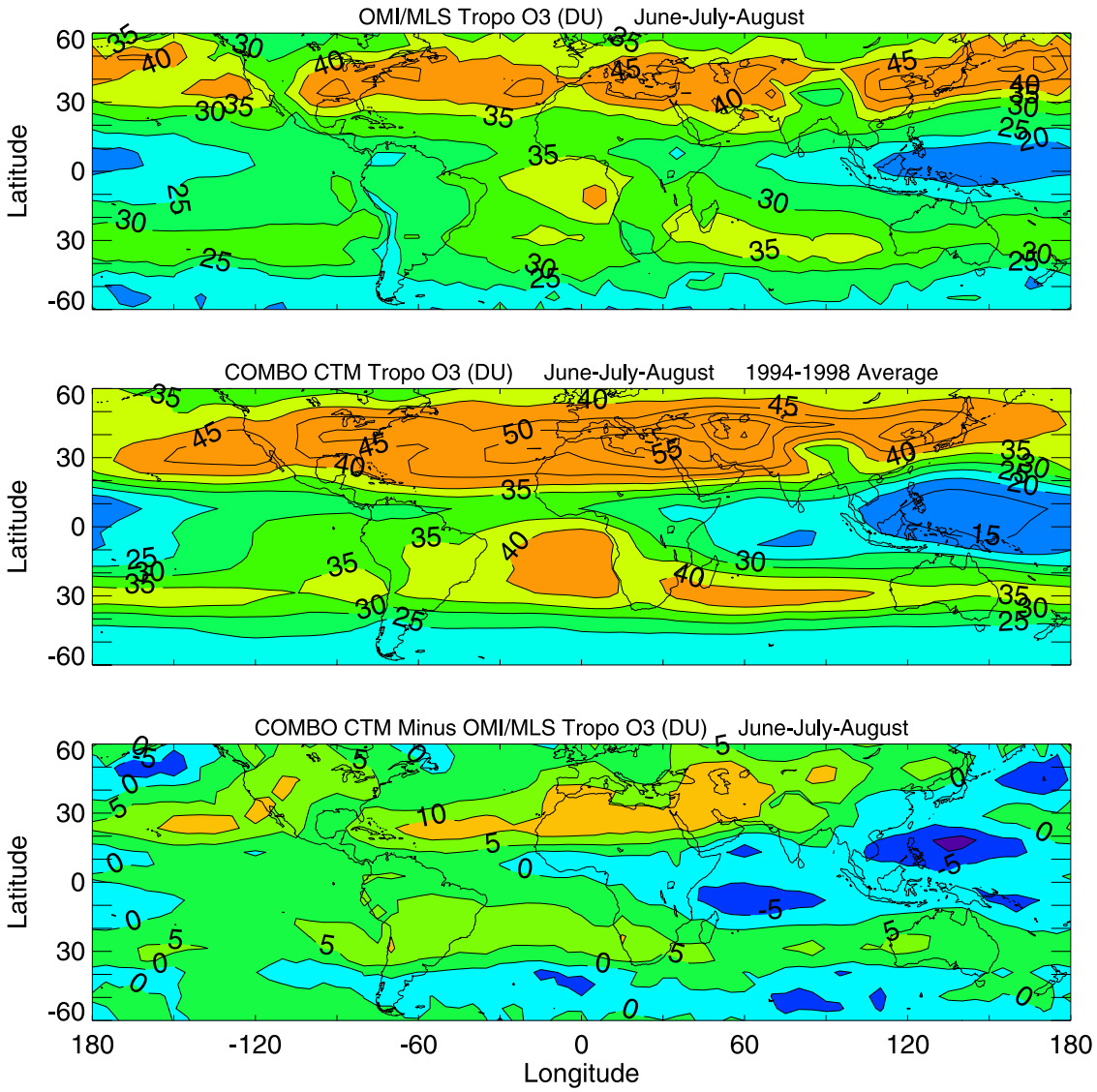

Figure 7d. Same as Figure 7a but for June–August.

Africa into the Atlantic Ocean, and also over Japan and the region of North America and to its west. The difference plot also indicates negative values in the Southern Hemisphere and the tropical western Pacific. Because of uncertainties present in both model and observed TCO values, differences of 10 DU and higher are subjectively interpreted as significant with smaller values considered essentially at noise level. In this respect, only yellow colored regions (>+10 DU) and purple regions (<−10 DU) in Figure 7a–7d (bottom) are considered significant. These regions represent only a small fraction of total surface area.

[37] The +10 DU band centered over northern Africa in Figure 7a (bottom) is a persistent feature of this region from June though October, and coincides in both pattern and seasonality with mineral dust from deserts in northern Africa (Sahara) and Saudi Arabia [e.g., *Torres et al.*, 2002; *Prospero and Lamb*, 2003]. Although the OMI version 8 ozone algorithm accounts for aerosols, the differences between OMI/MLS and the model may still be associated with errors in the OMI retrievals in the presence of desert dust. The +10 DU difference band could also be related to how desert dust is handled in the model. Differences of +10 DU over North America are not associated with desert dust and suggest a systematic offset present in northern latitudes between OMI/MLS and the model.

[38] For December–February (Figure 7b), both the observations and model show reductions in TCO in both hemispheres compared to September–November. These northern winter months show the smallest global mean ozone during the year. Figure 7b (bottom) indicates that regions in the Northern Hemisphere with differences greater than +10 DU are reduced compared to September–November. For March–May (Figure 7c) TCO values in the northern subtropics/midlatitudes reach 40–45 DU for both the model and measurements and are considerably larger than in the Southern Hemisphere. The differences between the model

Table 1. Calculated Spatial Statistical Parameters Between 2004–2005 OMI/MLS and 1994–1998 COMBO CTM TCO (in DU)[a]

Season	Latitude Band	OMI/MLS, DU	COMBO, DU	Difference, DU	RMS, DU	r
DJF	30–60°N	26.6	32.4	5.8	7.7	0.35
DJF	0–30°N	29.1	33.2	4.1	6.4	0.79
DJF	0–30°S	27.4	27.4	0.0	3.7	0.85
DJF	30–60°S	26.9	25.0	−1.9	4.8	0.84
MAM	30–60°N	33.2	39.7	6.5	7.5	0.65
MAM	0–30°N	33.4	35.5	2.2	5.4	0.88
MAM	0–30°S	25.7	27.2	1.5	4.0	0.82
MAM	30–60°S	24.9	24.7	−0.2	4.5	0.62
JJA	30–60°N	39.1	42.7	3.6	6.1	0.70
JJA	0–30°N	29.5	31.8	2.3	6.1	0.88
JJA	0–30°S	29.8	32.1	2.3	4.6	0.87
JJA	30–60°S	26.3	26.0	−0.3	2.9	0.84
SON	30–60°N	28.7	37.3	8.6	9.5	0.66
SON	0–30°N	27.6	30.3	2.8	6.3	0.76
SON	0–30°S	33.8	33.5	−0.3	3.1	0.92
SON	30–60°S	29.2	27.7	−1.5	4.7	0.76

[a]Mean values are given for the observations and model, mean differences (model minus observations), RMS of the differences, and correlations. Each 30° latitude band for each season (December–January–February (DJF), March–April–May (MAM), June–July–August (JJA), September–October–November (SON)) has a total of 432 colocated data pairs for statistical calculations.

and OMI/MLS TCO in March–May are less than 10 DU most everywhere.

[39] The model and observed TCO compare well in their basic features from June to August (Figure 7d), including the maximum over the Southern Hemisphere's tropical Atlantic Ocean, highest values in the Northern Hemisphere, and minimum ozone over the tropical maritime continent. Their differences are characterized by a +10 DU band extending from Saudi Arabia westward across northern Africa and the Atlantic Ocean. A similar band was noted previously for Figure 7a for September–November as being associated with desert dust. June–August coincide with the largest year-round concentrations of desert dust from Saudi Arabia and the Sahara desert of northern Africa. A large amount of the dust is transported westward across the Atlantic Ocean into the Caribbean [*Prospero and Lamb*, 2003].

[40] Table 1 provides a statistical summary of observed and modeled TCO in Figures 7a–7d. Table 1 lists spatially calculated statistical parameters in four 30°-latitude bands for each of the 3-month seasons. Listed are mean values, differences (COMBO CTM minus OMI/MLS), RMS of differences, and correlations. The numbers listed in Table 1 from the model's 5-year average are nearly identical when evaluated for individual years. In Table 1 the highest spatial correlations (up to 0.92) are in the 0–30°S band with mean offset differences at most of 2 DU and RMS values of ~4–5 DU. The excellent agreement in this latitude band is attributed to the ability of both observation and model in determining the large south Atlantic maximum and Pacific minimum in TCO. Overall, the model captures the spatial variability of OMI/MLS TCO in all latitude ranges except for the latitude band 30–60°N. In this latitude band, mean and RMS differences are largest, and correlations are smallest. (The largest difference (8.6 DU) is in September–November, and the smallest correlation (0.35) is in December–February). As discussed in section 5, the current model TCO is likely to be biased high in this latitude band because of too high stratosphere-to-troposphere flux of ozone.

[41] We compared seasonal patterns in TCO in Figures 7a–7d with seasonal patterns in TCO by *Fishman et al.* [1990], who combined several years (1979–1987) of SAGE stratospheric ozone measurements with Nimbus 7 TOMS total ozone. Despite the sparse measurements from SAGE, by averaging several years together *Fishman et al.* [1990] were able to evaluate global patterns and seasonal cycles in TOMS/SAGE TCO. Figure 9 of their study shows recognizable similarities in seasonal patterns in both hemispheres with OMI/MLS TCO and COMBO model TCO in Figure 7a–7d. More recently *Liu et al.* [2005] utilized a method to determine ozone profiles directly from GOME. In a follow-up application study, *Liu et al.* [2006] made 3-month seasonal maps of GOME TCO for years 1996–1997 (compare their Figure 6 with Figures 7a–7d in this study). In their Figure 6 they also included TCO maps from the GEOS-CHEM model. The basic features of patterns and seasonal cycles in TCO for GOME and GEOS-CHEM are similar to OMI/MLS and COMBO CTM. An advantage of the *Liu et al.* [2005] method is that tropospheric ozone can be determined using a single instrument, but as their study indicated the technique has difficulty for latitudes poleward of the subtropical wind jets (i.e., poleward of around ±30–35°) where around 50% of retrieved TCO comes from a priori ozone in the algorithm rather than measured ozone.

7. Daily Maps of OMI/MLS Tropospheric Ozone

[42] As a final topic we investigate the feasibility of obtaining daily maps of tropospheric ozone from OMI/MLS. Figure 8 shows two images of OMI/MLS ozone VMR over an entire hemisphere centered over the North Atlantic. In daily maps many pixel measurements are absent because of transient clouds. For this reason we have averaged daily maps over 5 days centered on 24 and 28 June in Figure 8 in effort to obtain as near global coverage as possible. The 5-day mean for 24 June shows high VMR (~75–80 ppbv) over the U.S. east coast compared to 28 June. For 28 June there is similar elevated ozone in

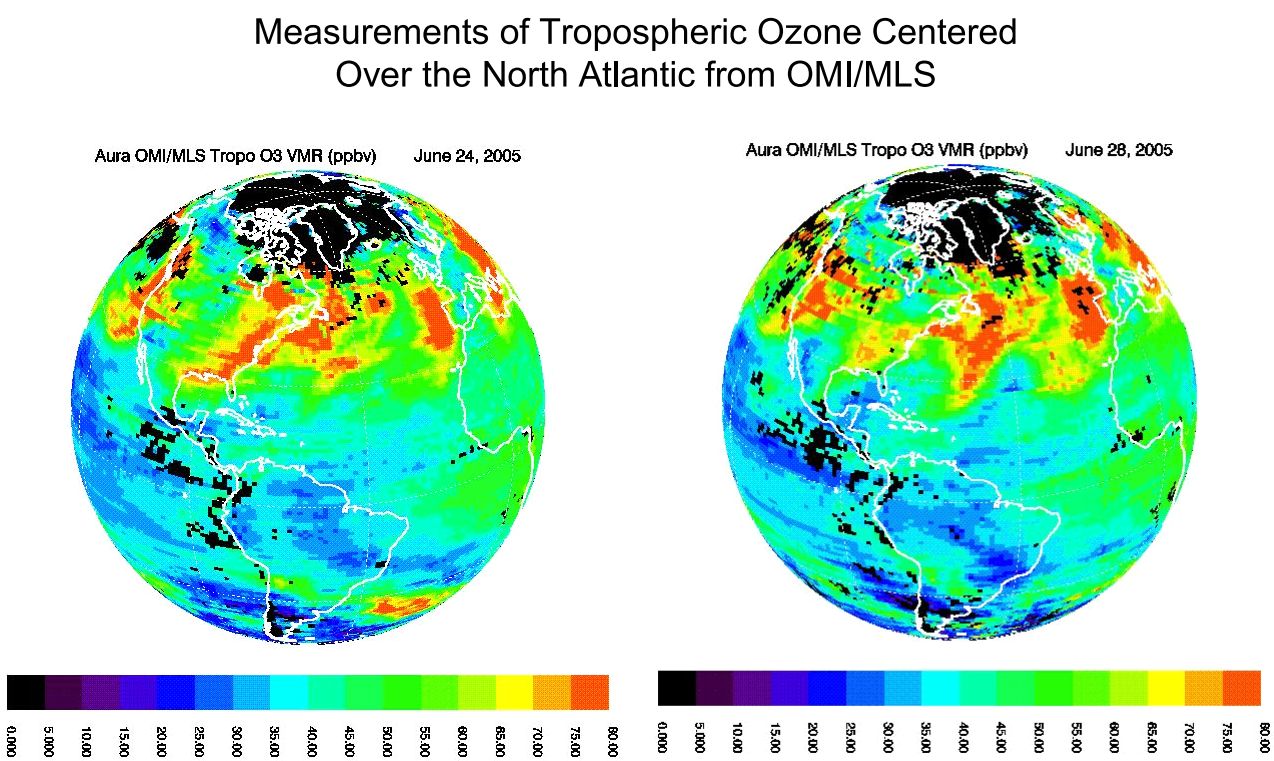

Figure 8. Two images of OMI/MLS ozone mean VMR over an entire hemisphere centered over the North Atlantic Ocean. Each image represents 5-day means centered about the date specified ((left) 24 June 2005 and (right) 28 June 2005). Color bars go from zero to 80 ppbv in steps of 5 ppbv.

the central North Atlantic region that may be related to eastward transport of east coast ozone from days earlier. Elevated ozone over the west coast of the U.S. for 24 June appears to have been transported eastward in the 28 June image. There are regions of enhanced ozone in eastern Europe and over the Atlantic Ocean west of Spain.

[43] Figure 8 suggests that the daily maps of OMI/MLS tropospheric ozone may be useful for tracking pollution events; however, the daily maps currently have difficulties. The impact of clouds in daily maps shields out many pixels of TCO and VMR from OMI/MLS. (A current plan (work in progress) is to invoke an extended algorithm which will allow TCO and VMR maps for cloudy pixel scenes from OMI/MLS.) Another potential problem for daily maps comes from the NCEP assimilated data (not an actual data measurement) which has several different definitions of tropopause pressure and contributes to additional errors in tropospheric ozone. For MLS, the current v1.5 retrievals have difficulty in accurately measuring ozone beyond 215 hPa; it is anticipated that the next MLS version will improve this condition. In addition, MLS measurements are along-track only and a method must be established to fill in data between orbital gaps to establish daily SCO maps. This study utilized a 2-D interpolation scheme to fill in missing MLS data. This study has also examined other methods including assimilation of MLS ozone (I. Stajner, personal communication, 2006). Another method is reverse domain filling (RDF) (M. Schoeberl, personal communication, 2006). These latter methods depend critically on the accuracy of wind fields and the vertical resolution and accuracy of the ozone profile measurements. All of these issues for improving the daily tropospheric ozone maps from OMI and MLS are being investigated as work in progress.

8. Summary

[44] One year (September 2004 to August 2005) of daily tropospheric ozone derived from Aura OMI and MLS measurements were evaluated for spatial and temporal variations and compared with the Global Modeling Initiative's COMBO CTM. OMI and MLS ozone retrievals indicate no substantial calibration differences for measuring tropospheric ozone as inferred from comparisons with both OMI CCD measurements of SCO and ozonesondes (WOUDC and SHADOZ) extending from the tropics to high latitudes.

[45] Monthly averaged OMI/MLS TCO was examined for month-to-month variability and global distributions. For September–November 2004, high values of ozone lie in the Southern Hemisphere in a large region extending from the equator in the Atlantic to 30–40°S along all longitudes. OMI/MLS measurements indicate local enhancements in TCO (>40 DU) over the Brazil Amazon region during these months of intense biomass burning. The OMI/MLS measurements for December 2004 to February 2005 show smallest global TCO. In March–May 2005 global TCO becomes larger with most concentration in the northern midlatitudes. In March–May in the northern midlatitudes, both land and oceanic regions have similar large ozone amounts (>40–45 DU). This is observed for July–August 2005 also. However, the largest TCO values (~45–50 DU) in July–August extend across two broad regions: (1) from

eastern Asia across the Atlantic Ocean and (2) over the Mediterranean region. The former for July was shown earlier by *Chandra et al.* [2004] in both observed TCO from EP TOMS/UARS MLS and the MOZART-2 model. The enhancement in the Mediterranean region in northern summer months was first described in the modeling study by *Lelieveld et al.* [2002]. The new OMI/MLS TCO measurements appear to confirm a Mediterranean "crossroads" effect.

[46] The basic features in TCO inferred from the first year of OMI/MLS measurements are well reproduced in a 5-year mean of TCO from the COMBO CTM. In regional assessments, both OMI/MLS and model TCO indicate lowest global values of tropospheric ozone (20 DU or less) year-round over the broad tropical Pacific and also in the southern polar region in summer and autumn months. The low values in the southern polar region are attributed to low values of ozone-producing photochemical sources and low influence from STE compared to other latitude regions. Despite the good agreement in basic features between OMI/MLS and model there are also noted differences. The largest differences between OMI/MLS and model TCO are around 10 DU but they represent generally small regions when evaluated globally. In the tropics persistent differences of 10 DU occur from June through October over northern Africa extending westward into the Atlantic. This feature coincides in both pattern and seasonality with mineral dust from the deserts in northern Africa (Sahara) and Saudi Arabia. The reason for this 10 DU discrepancy is not clear, but appears to be caused by desert dust affecting either OMI measurements or the model.

[47] It was shown that the maps of OMI/MLS tropospheric ozone have useful potential in tracking pollution events either regionally or globally, even though current daily measurements have known difficulties caused by both instrument retrievals and the residual technique used. The improvement of the daily global maps is a work in progress and is beyond the scope of the current investigation.

[48] **Acknowledgments.** Excellent support for this research has come from the Aura Project which is led by project scientist Mark Schoeberl and deputy project scientists Anne Douglass, Ernie Hilsenrath, and Joanna Joiner. The authors also thank the Aura MLS and OMI instrument and algorithm teams for the extensive satellite measurements used in this study. Thanks also go to Jack Fishman for helpful discussions regarding the OMI/MLS residual method. We acknowledge greatly the GMI team for their development and support of the COMBO CTM. We also appreciate the efforts of the SHADOZ science team for producing the SHADOZ ozonesonde data and also Bojan Bojkov for providing MLS data from the NASA Aura Validation Data Center. Funding for this research was provided in part by Goddard Earth Science Technology (GEST) grant NCC5-494.

References

Bey, I., et al. (2001), Global modeling of tropospheric chemistry with assimilated meteorology: Model description and evaluation, *J. Geophys. Res.*, *106*(D19), 23,073–23,095.

Bian, H., and M. J. Prather (2002), Fast-J2: Accurate simulation of stratospheric photolysis in global chemical models, *J. Atmos. Chem.*, *41*, 281–296.

Bloom, S., et al. (2005), Documentation and validation of the Goddard Earth Observing System (GEOS) Data Assimilation System–Version 4, *Tech. Rep. Ser. on Global Model. and Data Assim., NASA Tech. Memo. NASA/TM 104606*, vol. 26. (Available at http://gmao.gsfc.nasa.gov/systems/geos4)

Chandra, S., J. R. Ziemke, P. K. Bhartia, and R. V. Martin (2002), Tropical tropospheric ozone: Implications for dynamics and biomass burning, *J. Geophys. Res.*, *107*(D14), 4188, doi:10.1029/2001JD000447.

Chandra, S., J. R. Ziemke, and R. V. Martin (2003), Tropospheric ozone at tropical and middle latitudes derived from TOMS/MLS residual: Comparison with a global model, *J. Geophys. Res.*, *108*(D9), 4291, doi:10.1029/2002JD002912.

Chandra, S., J. R. Ziemke, X. Tie, and G. Brasseur (2004), Elevated ozone in the troposphere over the Atlantic and Pacific oceans in the Northern Hemisphere, *Geophys. Res. Lett.*, *31*, L23102, doi:10.1029/2004GL020821.

Chin, M., et al. (2002), Tropospheric aerosol optical thickness from the GOCART model and comparisons with satellite and sunphotometer measurements, *J. Atmos. Sci.*, *59*, 461–483.

Considine, D. B., et al. (2000), A polar stratospheric cloud parameterization for the three-dimensional model of the global modeling initiative and its response to stratospheric aircraft emissions, *J. Geophys. Res.*, *105*, 3955–3975.

Considine, D. B., et al. (2004), Simulating ozone in the near-tropopause region with a new combined model of the stratosphere and troposphere, paper presented at Quadrennial Ozone Symposium, Int. Ozone Comm., Kos, Greece, June.

Considine, D. B., et al. (2005), Sensitivity of Global Modeling Initiative chemistry and transport model simulations of radon-222 and lead-210 to input meteorological data, *Atmos. Chem. Phys. Disc.*, *5*, 5325–5372.

de Laat, A. T. J., I. Aben, and G. J. Roelofs (2005), A model perspective on total tropospheric O_3 column variability and implications for satellite observations, *J. Geophys. Res.*, *110*, D13303, doi:10.1029/2004JD005264.

Douglass, A. R., M. R. Schoeberl, R. B. Rood, and S. Pawson (2003), Evaluation of transport in the lower tropical stratosphere in a global chemistry and transport model, *J. Geophys. Res.*, *108*(D9), 4259, doi:10.1029/2002JD002696.

Douglass, A. R., R. S. Stolarski, S. E. Strahan, and P. S. Connell (2004), Radicals and reservoirs in the GMI chemistry and transport model: Comparison to measurements, *J. Geophys. Res.*, *109*, D16302, doi:10.1029/2004JD004632.

Duncan, B. N., R. V. Martin, A. C. Staudt, R. Yevich, and J. A. Logan (2003), Interannual and seasonal variability of biomass burning emissions constrained by satellite observations, *J. Geophys. Res.*, *108*(D2), 4100, doi:10.1029/2002JD002378.

Dunlea, E. J., and A. R. Ravishankara (2004), Kinetic studies of the reactions of $O(^1D)$ with several atmospheric molecules, *Phys. Chem. Chem. Phys.*, *6*, 2152–2161, doi:10.1039/b400247d.

Edwards, D. P., et al. (2003), Tropospheric ozone over the tropical Atlantic: A satellite perspective, *J. Geophys. Res.*, *108*(D8), 4237, doi:10.1029/2002JD002927.

Fishman, J., and J. C. Larsen (1987), Distribution of total ozone and stratospheric ozone in the tropics: Implications for the distribution of tropospheric ozone, *J. Geophys. Res.*, *92*, 6627–6634.

Fishman, J., C. E. Watson, J. C. Larsen, and J. A. Logan (1990), Distribution of tropospheric ozone determined from satellite data, *J. Geophys. Res.*, *95*(D4), 3599–3617.

Fishman, J., A. E. Wozniak, and J. K. Creilson (2003), Global distribution of tropospheric ozone from satellite measurements using the empirically corrected tropospheric ozone residual technique: Identification of the regional aspects of air pollution, *Atmos. Chem. Phys.*, *3*, 893–907.

Froidevaux, L., et al. (2006), Early validation analyses of atmospheric profiles from EOS MLS on the Aura satellite, *IEEE Trans. Geophys. Remote Sens.*, *44*(5), 1075–1092.

Hack, J. J. (1994), Parameterization of moist convection in the NCAR Community Climate Model, CCM2, *J. Geophys. Res.*, *99*, 5551–5568.

Jacobson, M. Z. (1995), Computation of global photochemistry with SMVGEAR II, *Atmos. Environ.*, *29*, 2541–2546.

Kinnison, D. E., et al. (2001), The Global Modeling Initiative Assessment Model: Application to high-speed civil transport perturbation, *J. Geophys. Res.*, *106*, 1693–1712.

Lelieveld, J., and F. J. Dentener (2000), What controls tropospheric ozone?, *J. Geophys. Res.*, *105*, 3531–3551.

Lelieveld, J., et al. (2002), Global air pollution crossroads over the Mediterranean, *Science*, *298*(5594), 794–799.

Levelt, P. F., et al. (2006a), The Ozone Monitoring Instrument, *IEEE Trans. Geophys. Remote Sens.*, *44*(5), 1093–1101.

Levelt, P. F., et al. (2006b), Science objectives of the Ozone Monitoring Instrument, *IEEE Trans. Geophys. Remote Sens.*, *44*(5), 1199–1208.

Lin, S.-J., and R. B. Rood (1996), Multidimensional flux-form semi-Lagrangian transport schemes, *Mon. Weather Rev.*, *124*, 2046–2070.

Liu, H., et al. (2001), Constraints from ^{210}Pb and ^{7}Be on wet deposition and transport in a global three-dimensional chemical tracer model driven by assimilated meteorological fields, *J. Geophys. Res.*, *106*, 12,109–12,128.

Liu, X., et al. (2005), Ozone profile and tropospheric ozone retrievals from the Global Ozone Monitoring Experiment: Algorithm description and validation, *J. Geophys. Res.*, *110*, D20307, doi:10.1029/2005JD006240.

Liu, X., et al. (2006), First directly-retrieved global distribution of tropospheric column ozone from GOME: Comparison with the GEOS-CHEM model, *J. Geophys. Res.*, *111*, D02308, doi:10.1029/2005JD006564.

Logan, J. (1999), An analysis of ozonesonde data for the troposphere: Recommendations for testing three-dimensional models and development of a gridded climatology for tropospheric ozone, *J. Geophys. Res.*, *104*, 16,115–16,150.

Martin, R. V., D. J. Jacob, J. A. Logan, J. R. Ziemke, and R. Washington (2000), Detection of a lightning influence on tropical tropospheric ozone, *Geophys. Res. Lett.*, *27*(11), 1639–1642.

Martin, R. V., et al. (2002), Interpretation of TOMS observations of tropical tropospheric ozone with a global model and in situ observations, *J. Geophys. Res.*, *107*(D18), 4351, doi:10.1029/2001JD001480.

Martin, R. V., et al. (2003), Global and regional decreases in tropospheric oxidants from photochemical effects of aerosols, *J. Geophys. Res.*, *108*(D3), 4097, doi:10.1029/2002JD002622.

Marufu, L., et al. (2000), Photochemistry of the African troposphere: Influence of biomass burning emission, *J. Geophys. Res.*, *105*, 14,513–14,530.

Moxim, W. J., and H. Levy II (2000), A model analysis of tropical South Atlantic Ocean tropospheric ozone maximum: The interaction of transport and chemistry, *J. Geophys. Res.*, *105*, 17,393–17,415.

Peters, W., M. Krol, F. Dentener, A. M. Thompson, and J. Lelieveld (2002), Chemistry-transport modeling of the satellite observed distribution of tropical tropospheric ozone, *Atmos. Chem. Phys.*, *2*, 103–120.

Pickering, K. E., Y. S. Wang, W. K. Tao, C. Price, and J. F. Muller (1998), Vertical distributions of lightning NO_x for use in regional and global chemical transport models, *J. Geophys. Res.*, *103*(D23), 31,203–31,216.

Price, C., and D. Rind (1992), A simple lightning parameterization for calculating global lightning distributions, *J. Geophys. Res.*, *97*(D9), 9919–9933.

Price, C., J. Penner, and M. Prather (1997), NO_x from lightning. 1. Global distribution based on lightning physics, *J. Geophys. Res.*, *102*(D5), 5929–5941.

Prospero, J. M., and P. J. Lamb (2003), African droughts and dust transport to the Caribbean: Climate change implications, *Science*, *302*(5647), 1024–1027.

Rasch, P. J., et al. (1997), Representations of transport, convection, and the hydrologic cycle in chemical transport models: Implications for the modeling of short-lived and soluble species, *J. Geophys. Res.*, *102*, 28,127–28,138.

Rotman, D. A., et al. (2001), Global Modeling Initiative assessment model: Model description, integration, and testing of the transport shell, *J. Geophys. Res.*, *106*, 1669–1691.

Schoeberl, M. R., et al. (2004), Earth observing systems benefit atmospheric research, *Eos Trans. AGU*, *85*, 177–178.

Schoeberl, M. R., B. N. Duncan, A. R. Douglass, J. Waters, N. Livesey, W. Read, and M. Filipiak (2006), The carbon monoxide tape recorder, *Geophys. Res. Lett.*, *33*, L12811, doi:10.1029/2006GL026178.

Shindell, D. T., et al. (2006), Multimodel simulations of carbon monoxide: Comparison with observations and projected near-future changes, *J. Geophys. Res.*, doi:10.1029/2006JD007100, in press.

Singh, H., et al. (2000), Distribution and fate of select oxygenated organic species in the troposphere and lower stratosphere over the Atlantic, *J. Geophys. Res.*, *105*, 3795–3805.

Stevenson, D. S., et al. (2006), Multimodel ensemble simulations of present-day and near-future tropospheric ozone, *J. Geophys. Res.*, *111*, D08301, doi:10.1029/2005JD006338.

Thompson, A. M., et al. (2003), Southern Hemisphere Additional Ozonesondes (SHADOZ) 1998–2000 tropical ozone climatology: 1. Comparison with Total Ozone Mapping Spectrometer (TOMS) and ground-based measurements, *J. Geophys. Res.*, *108*(D2), 8238, doi:10.1029/2001JD000967.

Torres, O., et al. (2002), A long-term record of aerosol optical depth from TOMS observations and comparison to AERONET measurements, *J. Atmos. Sci.*, *59*, 398–413.

Valks, P. J. M., R. B. A. Koelemeijer, M. van Weele, P. van Velthoven, J. P. F. Fortuin, and H. Kelder (2003), Variability in tropical tropospheric ozone: Analysis with Global Ozone Monitoring Experiment observations and a global model, *J. Geophys. Res.*, *108*(D11), 4328, doi:10.1029/2002JD002894.

van Noije, T. P. C., et al. (2006), Multi-model ensemble simulations of tropospheric NO_2 compared with GOME retrievals for the year 2000, *Atmos. Chem. Phys.*, *6*, 2943–2979.

Wang, Y., et al. (1998), Global simulation of tropospheric O_3–NO_x-hydrocarbon chemistry: 1. Model formulation, *J. Geophys. Res.*, *103*, 10,713–10,725.

Waters, J. W., et al. (2006), The Earth Observing System Microwave Limb Sounder (EOS MLS) on the Aura satellite, *IEEE Trans. Geosci. Remote Sens.*, *44*(5), 1075–1092.

Wesely, M., et al. (1985), Measurements and parameterization of particulate sulfur dry deposition over grass, *J. Geophys. Res.*, *90*, 2131–2143.

Wild, O., X. Zhu, and M. J. Prather (2000), Fast-J: Accurate simulation of in- and below-cloud photolysis in tropospheric chemical models, *J. Atmos. Chem.*, *37*, 245–282.

Zhang, G. J., and N. A. McFarlane (1995), Sensitivity of climate simulations to the parameterization of cumulus convection in the Canadian Climate Centre general circulation model, *Atmos. Ocean*, *33*, 407–446.

Ziemke, J. R., S. Chandra, and P. K. Bhartia (1998), Two new methods for deriving tropospheric column ozone from TOMS measurements: The assimilated UARS MLS/HALOE and convective-cloud differential techniques, *J. Geophys. Res.*, *103*, 22,115–22,127.

Ziemke, J. R., S. Chandra, and P. K. Bhartia (2001), "Cloud slicing": A new technique to derive upper tropospheric ozone from satellite measurements, *J. Geophys. Res.*, *106*, 9853–9867.

Ziemke, J. R., S. Chandra, and P. K. Bhartia (2005), A 25-year data record of atmospheric ozone in the Pacific from Total Ozone Mapping Spectrometer (TOMS cloud slicing: Implications for ozone trends in the stratosphere and troposphere, *J. Geophys. Res.*, *110*, D15105, doi:10.1029/2004JD005687.

P. K. Bhartia, NASA Goddard Space Flight Center, Code 613.3, Greenbelt, MD 20771, USA.

S. Chandra, B. N. Duncan, and J. R. Ziemke, Goddard Earth Sciences and Technology, University of Maryland Baltimore County, Baltimore, MD 21228, USA. (ziemke@jwocky.gsfc.nasa.gov)

L. Froidevaux and J. W. Waters, NASA Jet Propulsion Laboratory, Mail Stop 183-701, Pasadena, CA 91109, USA.

P. F. Levelt, Royal Netherlands Meteorological Institute, NL-3730 AE De Bilt, Netherlands.